

OPTICS RECYCLE LOOP STRATEGY FOR NIF OPERATIONS ABOVE UV LASER-INDUCED DAMAGE THRESHOLD

M. L. Spaeth,¹ P. J. Wegner,^{1*} T. I. Suratwala,¹ M. C. Nostrand,¹ J. D. Bude,¹ A. D. Conder,¹
J.A. Folta,¹ J. E. Heebner,¹ L.M. Kegelmeyer,¹ B. J. MacGowan,¹ D. C. Mason,¹ M. J.
Matthews,¹ and P. K. Whitman¹

¹ Lawrence Livermore National Laboratory, Livermore, CA

Contact: Paul Wegner
Lawrence Livermore National Laboratory
7000 East Avenue, L-580
Livermore, CA 94550
925-423-2483
wegner1@llnl.gov

Total number of pages: 95

Total number of tables: 2

Total number of figures: 30

LLNL-JRNL-658260

OPTICS RECYCLE LOOP STRATEGY FOR NIF OPERATIONS ABOVE UV LASER-INDUCED DAMAGE THRESHOLD

M. L. Spaeth,¹ P. J. Wegner,^{1*} T. I. Suratwala,¹ M. C. Nostrand,¹ J. D. Bude,¹ A. D. Conder,¹ J.A. Folta,¹ J. E. Heebner,¹ L.M. Kegelmeyer,¹ B. J. MacGowan,¹ D. C. Mason,¹ M. J. Matthews,¹ and P. K. Whitman¹

¹ Lawrence Livermore National Laboratory, Livermore, CA

*Corresponding author: wegner1@llnl.gov

ABSTRACT

The National Ignition Facility (NIF) at Lawrence Livermore National Laboratory houses the world's largest laser system, composed of 192 individual, 40-cm-aperture beamlines. The NIF laser routinely operates at ultra-violet (UV) fluences above 8 J/cm^2 , roughly twice the damage threshold of commercially available UV-grade fused silica. NIF is able to maintain such high fluence operation by using an optics recycling loop strategy. Successful operation of the loop relies on a number of technologies specifically developed for NIF. One of the most important is the LLNL- and vendor-developed capability for producing highly damage-resistant optics. Other technologies developed for the Optics Recycle Loop raise the operating point of NIF by keeping damage growth in check. LLNL has demonstrated the capability to sustain UV fused silica optic recycling rates of up to 40 optics per week. The optics are ready for reinstallation after a three-week trip through a recycle "loop" where the damage state of each optic is assessed and repaired. The impact of the optics recycle loop has been profound, allowing the experimental program to routinely employ energies and fluences that would have been otherwise unachievable. Without the recycle loop, it is likely that the NIF fluence would need to be kept

below the UV threshold for damage growth, $\sim 4 \text{ J/cm}^2$, thus keeping the energy delivered to the target significantly below 1 MJ. With the recycle loop implemented during the National Ignition Campaign, NIF can routinely deliver $>1.8 \text{ MJ}$ on target, an increase in operational capability of close to 100%. In this review, the enabling technological advances, optical performance, and operational capability implications of the optics recycle loop are discussed.

Keywords: Lasers and laser optics; laser damage; lasers, pulsed; UV lasers.

This work performed under the auspices of the U.S. Department of Energy by Lawrence Livermore National Laboratory (LLNL) under Contract DE-AC52-07NA27344.

LLNL-JRNL-658260

ACRONYM GLOSSARY

1 ω	fundamental neodymium: glass laser frequency (1.053 μm wavelength)
3 ω	third harmonic laser frequency (0.351 μm wavelength)
AMP	advanced mitigation process
BOE	buffered oxide etch
CCD	charge-coupled device
FICS	flaw identification and characterization station
FLRT	flaw removal tool
FOA	final optics assembly
FODI	final optics damage inspection
GDS	grating debris shield
HED	high energy density
ICF	inertial confinement fusion
IOM	integrated optics module
LCoS	liquid crystal on silicon
LLNL	Lawrence Livermore National Laboratory
LRU	line-replaceable unit
MRF	magneto-rheological finishing
NIC	National Ignition Campaign
NIF	National Ignition Facility

OALV	optically addressable light valve
OMF	optics mitigation facility
PAM	pre-amplifier module
PROP	LLNL laser propagation model
PSDI	phase-shifting diffraction interferometer
PSS	programmable spatial shapers
UV	ultraviolet
WFL	wedged focus lens

I. INTRODUCTION

I.A. NIF History and Laser Damage Requirements

For many years, scientists and engineers at U.S. national laboratories have been interested in creating a laser facility able to study the extreme temperature and density conditions, or high-energy-density (HED) physics, that are present in stars and in an exploding thermonuclear device. By the early 1970s, facility designers at Lawrence Livermore National Laboratory (LLNL) had concluded that the laser concept most likely to meet these far-reaching goals would be based on neodymium (Nd):glass. The laser would first generate high-energy, high-power pulses in the near-infrared, at a 1ω frequency, followed by frequency conversion of this light into the near-ultraviolet (UV), at 3ω .

The top-level design requirements for the National Ignition Facility (NIF) called for a pulsed laser capable of delivering a total on-target energy of 1.8 MJ, with a total peak power of 500 TW in the UV. In addition, 192 beams needed to be delivered in four cones to a small target located at the center of a 5-m-radius target chamber. The edge length of each nominally square beam is ~ 37 cm (within a 40 cm hard aperture), with a total effective area per beam of $\sim 1,240$ cm^2 . Accounting for transport losses between the final focus lens and the target, the average UV fluence at the lens (J/cm^2) for each beam was calculated to range from 8 to 9 J/cm^2 , with a spatial average peak intensity of ~ 2.3 to 2.5 GW/cm^2 .

As illustrated in Fig. 1, the requirements for the NIF laser would make it unique compared to the earlier 3ω lasers built to study HED science: e.g., the OMEGA laser at the University of Rochester's Laboratory for Laser Energetics and the Nova laser at LLNL. These inertial confinement fusion (ICF) lasers typically operated with a fluence of about one third of their design point. NIF would instead need to operate at about 12 times the fluence of those pre-

existing facilities. In addition, because of the large increase in total required energy, the total area of the optics in the 192 beams would be scaled upward by a factor of ~8.

When engineering and environmental studies for the NIF laser were beginning, studies of small samples indicated that the threshold fluence for laser damage initiation was $>14 \text{ J/cm}^2$ at NIF-relevant pulse formats, well above the $8\text{--}9 \text{ J/cm}^2$ requirement.¹ At the time, it was believed that bringing the performance of large optics up to the levels demonstrated for small samples would be relatively straightforward. The probabilistic nature of damage initiation was not yet understood. In addition, the concept that would later become known as "damage growth" was yet to be discovered.

NIF construction began in 1997 and was well under way in 1999 when two concepts related to laser damage of optics came to be understood at a basic level. First, researchers found that surface damage initiation is not a threshold event. Rather, it can be described as the probability of finding a number of damage sites per unit area of an optic as a function of the incident 3ω fluence on that optic.² This result meant that bringing the performance of large-area optics up to that demonstrated for small samples would likely be much more challenging than previously thought. Second, once a damage site has been initiated, it can grow to a larger size, and growth is exponential with the total incident fluence.³ In addition, results showed that the fluence threshold for damage growth is approximately 4 J/cm^2 , significantly less than the required operating fluence for NIF.

As shown in Fig. 2(a), when damage sites first initiate under the high fluence levels of NIF, the diameter of the sites is very small, varying from 5 to 30 μm . Sites of this size would not be a problem for continued laser operation if they remained small. However, because continued illumination of fused silica optics at NIF fluences is likely to result in quite rapid site growth

with every shot, this growth will continue until the optic becomes unusable for experiments. An example of site growth is shown in Fig. 2(b).

By 2001, the dilemma facing NIF had become very clear. It was imperative that NIF operate between 8 and 9 J/cm². Unfortunately, available optics and processes were not going to reach this range. The fused silica optics then available would form greater than ~17,000 damage sites per optic at the required NIF operating fluence. After 10 shots or so, the optic would no longer be usable. Operating costs introduced by this situation would prohibit sustained use of the facility.

Addressing these issues involved two initiatives: (1) a science-based approach for making fused silica optics more resistant to damage initiation, and (2) development of an optics recycle loop strategy and its supporting technologies to reduce time and costs involved in replacing and repairing optics. Figure 3 shows the recycle loop for the 3 ω optics. Functions in yellow represent steps associated with making optics that are resistant to damage initiation; Section II.A discusses the dramatic improvements made in this area since 2001. The remaining functions (in blue) relate to steps and decision points necessary for maintaining routine laser operation.

I.B. Overview of Optics Recycle Loop Operation

The NIF optics recycle loop is designed to service the 3 ω fused silica optics deployed in the NIF final optics assemblies (FOAs, see Fig. 4). Like other activities associated with refurbishment, the recycle loop requires the convenient and efficient handling of the refurbished parts, both for installation and removal from the laser and for moving through the various processing and inspection stations. Ensuring a convenient, efficient process meant designing light-weight line-replaceable units (LRUs) for the final optics: structures consisting of an

individual optic and its frame. During transportation between processing stations, the LRUs are held in clean mini-environments called “loop cases” that are designed to dock with the FOA during installation and removal, and with other key hardware along the loop path. The LRU hardware includes kinematic mounts that allow for rapid, pre-aligned installation into the integrated optics module (IOM). The hardware also holds small optics for coupling edge-illumination light into the optic during in-situ damage inspection.

The optics recycle loop is a nested assembly of loops with decision points for moving from one loop to another. With state-of-the-art, damage-resistant optics in place (Section II.A), the innermost loop allows the laser to be fired repeatedly. Shots with fluence or intensity on the 3ω optics that is high enough to be of damage concern are followed by in-situ optics inspection using the final optics damage inspection (FODI) system, which can be placed at the center of the target chamber center between shots (Section II.B). FODI can inspect the damage on individual optics, and the FODI companion optics inspection software can track the nominal size of growing sites. The innermost loop can continue to operate until the size of any inspected site is such that action is needed to prevent that site from growing to an unreparable size (greater than $\sim 300 \mu\text{m}$, Section II.E). At that point, if the operating configuration of the laser allows, a small spot blocker generated by a programmable spatial shaper (PSS) can be electronically placed in the low-energy and low-power beam path of the preamplifier module for the quad containing the laser beam of interest to shadow the damage site and prevent further growth (Section II.C). Information describing the location where the PSS should place the shadow to protect the damage site is provided by the FODI and optics inspection system. With a spot blocker in place, the laser can then be fired again, with continued optics inspection between shots that have fluence high enough to cause significant growth. Additional spot blockers can be added as

additional growing sites are identified. When the beam area covered by multiple shadows becomes a significant fraction of the total beam area, it will impact the energy that can be delivered. At that time, one or more optics in the affected quad must be removed and exchanged with a new or recycled (i.e., repaired) optic.

Damage site data is continually analyzed to determine when sites should be blocked and when optics should be removed. Damage growth models predict the increase in the size of a site that is likely to result from future scheduled laser shots. The size and location of every shadow is fed to the laser performance operation model so that subsequent firing of the laser can account for them. Other models are used to optimize the optic exchange plan and efficiently maintain the overall health of the laser.

When, according to the optics exchange plan, it is time for a particular optic to be replaced, it is removed from the laser (Fig. 5) and transported via loop case to a facility located adjacent to the target bay. There, the optic is surveyed for tritium and other hazardous contaminants that it may have been exposed to on the target chamber and, if necessary, decontaminated. It is then transported to the optics processing facility, where it is disassembled from the LRU frame. Next, the optic is passed through an automated cleaning system that uses aqueous solutions to strip the sol-gel anti-reflection coating from the optic, precision clean it, and rinse it with deionized water. The cleaned optic is then inspected to assess its recyclability in terms of surface quality, surface damage, and deeper bulk damage.

When optics reach a damage state that cannot be mitigated at LLNL, they are returned to the vendor for refinishing (the outer loop of Fig. 3), or discarded and replaced with a new optic. Optics suitable for reuse receive a new anti-reflection coating^{6, 7, 8, 9} and are screened on a flaw identification and characterization station (FICS). The FICS (Fig. 6) is designed to locate

process-induced optical flaws, such as those introduced during the finishing or coating processes. The FICS flaw maps are combined with the FODI damage maps obtained on the target chamber to provide a complete list of sites for further investigation. Sites that require detailed characterization prior to making a decision regarding their possible mitigation are further characterized on FICS with a phase-shifting diffraction interferometer (PSDI), which uses 532-nm light to measure the phase and amplitude modulation introduced by a flaw with better than 1/100 wave resolution.^{10, 11} The phase and amplitude data is automatically processed with an optical propagation code, similar to that employed for the original design of NIF, to calculate the downstream modulation that would be introduced by the flaw if it were placed at the planned location. The software uses rules based on damage initiation probability to judge whether the modulation introduced by each flaw would be acceptable. In this way, a short list of process-induced flaws that require mitigation is created. Flaws that fail the acceptance testing are removed either by stripping the entire optic and re-applying the anti-reflection coating, or by localized removal of the flaw with a flaw removal tool (FLRT).¹²

After the FICS test is completed, the optic is reassembled into an LRU and transported to the optics mitigation facility (OMF), where its damage sites undergo localized repair using a focused CO₂ laser (Fig. 7). The OMF systems also provide microscopic inspection of the candidate sites to classify the flaw, assign a mitigation protocol, and confirm that mitigation has been successful. Typical processing times for damage repair are four to six hours per optic. Each optic then receives a final quality assurance inspection with a bright light in a dark room, where a skilled operator identifies physical damage, scratches, coating scuffs, and cleanliness. Orientation of the optic within the LRU frame and proper assembly of the LRU hardware is also

verified at this time. The refurbished ready-to-install optic is then shipped to NIF, where it is stored under clean, dry-air purge conditions until it is needed.

The complete recycle process takes approximately three weeks and is mostly limited by wait-time at production work centers already populated with work-in-process optics. The process could be performed in a single week if an optic were given top priority at every step. The rate-limiting production steps are typically strip cleaning, FICS metrology, and damage mitigation, so multiple machines are provided for these areas to achieve the required capacity and reduce the risk of single-point equipment failures. The capacity of the recycle loop can be quite high: by the end of 2012, it was operating at a sustainable throughput of 40 optics per week. This capacity and cycle time provided by the recycle loop are both roughly an order of magnitude beyond that available from the optics finishing industry.

All of the optics recycle loop facilities and their specially built equipment are unique in the world. No other high-energy laser facility has taken up the challenge of operating above the damage initiation limit of commercially available optics and above the damage growth threshold for fused silica.

II. ENABLING TECHNOLOGIES FOR THE RECYCLING LOOP

In 2001, with the concepts for the optics recycle loop in place, it was becoming apparent that a number of new capabilities would need to be developed for the loop to operate effectively. These capabilities, together with the concept of programmable spot blocking developed in 2006, comprise the enabling technologies for the optics recycle loop that will be described in the following sections:

- Optics that are resistant to damage initiation—the more resistant, the better (Section II.A)

- An in-situ ability to measure the location and size of damage sites on each optic (Section II.B)
- The electronic ability to block incident light on a growing damage site (Section II.C)
- The mechanical and clean-handling ability to rapidly remove and replace a damaged optic (Section II.D)
- The ability to repair a damage site while meeting stringent specifications regarding the characteristics of the repaired site and the processing necessary for bringing the entire optic back to a near-perfect condition (Section II.E).

By far the most significant of these enabling technologies is damage-resistant optics. By 2001, operational systems analysis had identified a goal of allowing no more than 10 precursor sites on an optic to be installed on NIF. Energetics and microscopic studies had led to a hypothesis that very small damage precursors were associated with microfractures (cracks) located within less than $\sim 1 \mu\text{m}$ of the surface. As described in the following section, aggressive pursuit of finishing improvements between 2001 and 2007 reduced the anticipated number of sites per optic at the specified NIF design fluence from $\sim 17,000$ (on 1997-era optics) down to ~ 90 . Although this reduction was extremely important, 90 precursor sites per installed optic was still higher than acceptable.

In the meantime, parallel work had led to an improved understanding of the nature of damage initiation.¹³ Precursors lead to damage because, although they are very small, they are very effective at absorbing incident laser light and can locally reach high temperatures. Heat generated at their locations can then diffuse into the surrounding bulk material. When the temperature of bulk fused silica goes above $\sim 5000^\circ\text{C}$, the bulk material itself becomes absorbing at 3ω , leading to local run-away heating that continues until the laser pulse is over. Our model

that describes the dependence of damage initiation on pulse length and shape (called Equivinit) is based on thermal diffusion.¹⁴ In this paper, all fluences associated with damage initiation are quoted at their 3-ns Gaussian pulse equivalent.

One technique that was pursued for a number of years to reduce the number of precursors on a “finished” optic was pre-initiation, followed by repair of the pre-initiated sites.¹⁵ In fact, until ~2007, the only means for identifying the location of damage precursors was by their damage initiation. By 2005, it was recognized that a technique for nondestructive identification of damage precursors was needed to form the basis for continued reductions in finishing introduced precursors. Between 1997 and 2000, LLNL pursued a number of nondestructive test methods, but none of those studied provided high-confidence results. Pursuit of a nondestructive method was re-initiated in 2006, and led to the high-confidence technique known as “fast photoluminescence,” in which the signature of damage precursors was found to be luminescence with a continuum of lifetimes ranging from <50 ps to 5 ns.¹⁶ This important advance set the stage for an additional ~100× improvement in the damage resistance of fused silica optics through the advanced mitigation process (AMP) (described in the finishing section).

Between 2008 and 2012, the NIF laser was steadily brought up to routine operation at increasing energy and power levels as the new damage-resistant optics and full recycling capability were made available. That the loop is successfully supporting NIF was demonstrated in the late summer of 2012, when the laser delivered over 1.8 MJ on target at a peak power of over 500 TW, corresponding to an average fluence of 10 J/cm² in the FOA when scaled to 3 ns; this is well beyond the original design goal of 8 to 9 J/cm².

II.A. Damage-Resistant 3ω Optics

II.A.1. Optical Finishing

Economical operation of the loop requires that the number of damage sites expected to be initiated by the laser on a newly installed optic be on the order of tens of sites or less.

Historically, the dominant location for laser damage initiations on ICF lasers has been the fused silica optical surfaces exposed to 3ω laser light. Therefore, improvements in surface preparation processes such as finishing (grinding and polishing) and post-processing (cleaning, etching, and coating application) have been areas of active research. For typical production finishing processes in 1997, the number of laser damage initiations observed on fused silica optics was $\sim 15/\text{cm}^2$ ($\sim 17,000$ per NIF-sized optic) when exposed to the NIF 3ω design fluence of $8 \text{ J}/\text{cm}^2$ (see Fig. 8). By 2007, the number of initiations had been reduced to $\sim 0.08/\text{cm}^2$ ($\sim 90/\text{optic}$). This dramatic improvement is largely the result of work on improved finishing processes—more specifically, to the reduction of surface microfractures (or scratches), which are now known to be absorbing precursors and a host for absorbing precursors leading to laser damage.^{17, 18} During this period, a science-based program on understanding finishing, particularly on characterizing the fracture mechanics and tribology involved in the creation of surface microfractures, was an important aid in developing these new finishing processes.

A typical finishing process of glass optics begins with grinding, during which material is removed rapidly (at a rate of $10\text{--}10,000 \text{ }\mu\text{m}/\text{hr}$) by applying an ensemble of highly loaded particles to produce a high density of intersecting surface microfractures. Grinding is followed by polishing, a process in which material is removed more slowly (at $0.05\text{--}5 \text{ }\mu\text{m}/\text{hr}$) by inducing a chemical reaction or plastic flow using smaller particles at relatively low loads. It is particularly important to focus on controlling the grinding process because this step creates the high areal density of small microfractures that can later become laser damage precursors. The

microfractures from grinding must be removed in subsequent finishing steps to achieve highly damage-resistant surfaces. The standard finishing strategy has been to remove the microfractures created in one grinding step during the following grinding step by applying smaller abrasives that reduce microfracture depth. A new quantitative and statistical diagnostic of the microfracture depth distribution, called the magneto-rheological finishing (MRF) wedge technique, greatly aided in quantifying the quality of a given grinding process and in determining more precisely how much material should be removed in one step to eliminate all residual microfractures created in the previous step.^{19, 20, 21} Figure 9(a) shows typical microfracture depth distributions measured using the MRF wedge technique; notice that statistics are obtained down to 1 of 10^6 fractures. These depth distributions were explained using a model in which an ensemble of loaded particles at the workpiece/lap interface had varying loads/particle proportional to particle size, which leads to varying crack depths (derived from fracture mechanic and tribology relationships of sliding Hertzian indentation with friction).^{19, 22, 23} The predictions from this model and supporting experimental data illustrate the importance of using a grit (i.e., particles) for each grinding step that have little or no oversized particles. Even a minute amount of larger particle contamination in the abrasive particle size distribution can dramatically increase the depth distribution of damage¹⁹⁻²⁴; hence, rogue abrasive particles or asperities must be carefully controlled during the grinding process.

During polishing, where the final surface figure and roughness are achieved, material removal from the in-work optic is dominated by a chemical or plastic flow mechanism. Here also, the presence of rogue particles (particles noticeably larger than the mean particle size of the polishing slurry) can lead to higher loads/particle, which will initiate fracture formation i.e., scratches (see Fig. 9(b)).²⁴ Polishing scratches are typically composed of a series of

microfractures, called trailing indent fractures, which have a periodic spacing along the scratch length. Just as for grinding, the strategy for reducing scratches during polishing has led to improved management or reduction of rogue particles. Sources of rogue particles include particles from the environment, oversize particles in the size distribution of the initial slurry, and the changes to particle-size distribution during polishing—for example creation of dried slurry agglomerates or chemistry-induced agglomeration. A number of techniques have been applied to minimize the presence of rogue particles, including slurry filtration, improved slurry chemistry, environmental enclosures, and improved polisher housekeeping.^{25, 26} A variety of full- and sub-aperture polishing processes are available, including various pad and pitch polishing as well as MRF and bladder polishing. Some techniques, such as MRF, are less prone to interactions with rogue particles due to reduced normal loads²⁷; however, any technique, in principle, can achieve few or no microfractures by reducing or eliminating rogue particles.

Chemical etching processes have also been found to aid in improving the finishing process. On a polished surface, many fine scratches are covered by a thin (typically 70 nm) hydrated layer, called the Bielby layer, making them very difficult to identify using standard inspection techniques.²⁸ A short hydrogen-fluoride (HF)-based etch of the optic removes the Bielby layer and opens the scratches so they are much easier to diagnose. Inspections made during and at the end of the finishing process are compared with derived relationships between scratch width and scratch depth, to determine if any existing scratches would be removed in subsequent fabrication steps or should be removed by repeating earlier steps in the process.^{19, 24,}
²⁹ In addition, useful forensic rules were developed to determine the cause of an observed scratch, making it possible for the source of the rogue particles to be identified and mitigated.^{19,}
^{24, 29} Chemical etching can also reduce polishing time. Immediately after the grinding process,

the surface will have a high density of microfractures, which would take a long time to remove by polishing alone. With a longer HF-based etch following the grinding step, neighboring microfractures open up and are annihilated; this etch step reduces the depth of the initial fracture damage by up to three times²⁸ and thus reduces the amount of polishing time needed to remove the grinding layer.

With these advancements, the finishing-induced scratch count per optic dropped dramatically between 1997 and 2007 (Fig. 10), resulting in the similarly dramatic reduction in number density of laser damage initiations shown in Fig. 8. However, 90 initiations per optic remained too high for practical use of the optics recycle loop, requiring development of further mitigation strategies (Section II.A.2).

Finishing research and development has continued post-2007 to reduce the finer plastic-type scratches (leading to smoother surfaces) for improved optical performance with lower scatter and less damage, and to develop novel polishing methods that will reduce the cost of finishing while maintaining the high surface quality.^{25, 26, 30-36} For example, a recently developed polishing method, called convergent polishing, is capable of rapidly finishing flat and spherical glass optics in a single iteration, regardless of the initial surface figure of the workpiece.^{25, 26, 33-35} This process also leads to excellent surface quality under a fixed set of polishing parameters, workpiece after workpiece. In contrast, conventional full-aperture polishing methods require multiple, often long, iterative cycles (performed by a highly skilled optician) involving polishing, metrology, and process change to achieve the desired surface figure and surface quality.

II.A.2. Chemical Treatment

One possible path to reducing damage beyond the 2007 levels is to continue to reduce surface flaws, either through polishing or improved handling procedures. Although work continues toward this end, in practical terms, eliminating fractures is extremely difficult.

Another approach—and a key step in further reducing the number of precursor sites on fused silica optics—was the development of a post-finishing whole-optic chemical treatment process designated AMP2.^{37,38} Referring to Fig. 8, AMP2 takes a well-finished optic having about 90 initiations at 1.8-MJ NIF energies and improves it to less than five initiations per optic,³⁸ a dramatic and enabling development for practical implementation of the optics recycle loop strategy. Development of the AMP2 capability was made possible by the fast-photoluminescence nondestructive diagnostic described earlier. This diagnostic allowed NIF researchers to focus effort on understanding *why* surface fractures lead to damage and to identify the most important silica damage precursors below 10 J/cm². Using the fast-photoluminescence diagnostic to examine microfractures introduced during grinding and polishing merged the understanding described in Section II.A.1 with the parallel concerted effort to understand the physics of the damage process.^{13, 17, 18, 39, 40}

Studying the photoluminescence of microfracture defects created in a controlled way (and similar to those created during finishing) led to important clues about the nature of precursors. Their fast photoluminescence decay times suggest a large amount of disorder and high defect density.^{18,39} This same type of behavior was also found near the surface of a finished optic. Polishing is known to affect the surface in ways that create defects in glass, for example, through plastic material flow, densification of near-surface glass, and at higher stresses, fractures themselves.⁴⁰ Hypotheses for why surface fractures are associated with damage precursors include:

- Microfractures might act as a trap for absorbing impurities.
- The surfaces of microfractures might be an inherent source of sub-band gap absorbers.
- Microfractures might lead to significant electric field intensification.^{41, 42}

Surface micro-indentation was performed to generate flaws with all of these structural defects by controlling the indentation load and using a variety of indenters.¹⁷ Various elements of the flaws were then isolated by mechanical and chemical means; for example, fractured and plastically deformed regions were removed by MRF, fracture-free regions were created with Knoop indenters, and large fractures were created with high loads and diamond-tip indenters.²² Each indent was characterized using the fast-photoluminescence diagnostic, and damage tests were performed to measure the corresponding damage thresholds. Damage precursors were clearly associated with fractures, but not with the other features. Cross-sectional images of the fast photoluminescence of these defects showed that the absorbing precursors were within several hundred nanometers of the fractures' surface. To determine how deep these defects extended, we chemically etched the shallowest indents with HF:NH₄F acid, or buffered oxide etch (BOE). A 100-nm etch removed the photoluminescence signal and increased the local damage threshold from 7 J/cm² to over 20 J/cm². Since the chemical etching did not remove the fracture, the improvement in damage resistance could not be attributed to a reduction of optical intensification in the fracture. This finding, together with the removal of the defect photoluminescence, clearly associated damage precursors with a very thin defect layer on the fracture surface.¹⁷

Because these defect layers can be chemically etched away, a whole-optic etch process was utilized to remove the presence of damage precursors. For a small fracture, a 100-nm etch was sufficient, but this shallow etch did not improve the damage threshold of larger and deeper

fractures. A longer etch was required to open deeper fractures so that the etchant could reach the fracture tips and remove the defect layer from the entire fracture surfaces. However, as the etching depth increased, precursors reappeared, which again reduced the damage threshold. These new precursors were found to be associated with etch-related precipitates that preferentially formed on the fracture surfaces and cusps. The precipitates are likely salts of the hexafluorosilicate ion produced while etching. Understanding the concept that etch byproducts could be re-deposited in scratches to become new damage precursors was a key finding both for solving a mystery of mixed results found for previous etching attempts and for defining a path for developing a whole-optic etching process.

Next, a systematic investigation was performed of aqueous fluoride-based etching with the goal of reducing re-deposition and increasing the damage threshold of fractures with widths up to 30 μm .^{37, 38} Fused silica plates were polished and then scratched in a deterministic manner by passing them over a pad containing 200 μm silica spheres. The scratches produced in this way were typical of the brittle, trailing indent scratches found on high-quality polished optics (Fig. 9(b)). The test samples were etched with various HF-based etchants and under a variety of conditions that were considered effective in suppressing re-deposits. A chemical solubility and mass-transport-etching model was developed to guide the search for optimal etch and rinsing conditions. The model utilized both a moving boundary, to account for the change in crack geometry during etching, and diffusion and advection mass transport, to predict reaction product concentration profiles (and ultimately precipitation) within and around the crack during etching, rinsing, and drying. Finally, damage tests were performed on the treated scratches to determine damage thresholds as a function of scratch width. Some of the variables investigated included etch removal, static and ultrasonic agitation in the rinse bath, and BOE composition.

Figure 11(a) shows data collected from this study.³⁸ The data shows that non-etched scratches wider than a few micrometers begin to damage strongly; scratches wider than 5 μm would be expected to damage under typical NIF operating conditions. Consistent with the indent study described above, a shallow, static BOE etch can mitigate scratches below about 5 μm in width but is ineffective for wider scratches. Ultrasonic agitation of the etch bath provides a better removal of etch products and, hence, a lower probability of precipitation. It can more effectively treat wider scratches, but is still not very effective on scratches wider than 20 μm (series C). Another way to reduce the probability of precipitation is to reduce the relative concentration of ammonium fluoride in the buffered etch solution; the data of series D shows that the probability improves from 20:1 BOE with the original (higher) ammonium fluoride ion concentration to 6:1 BOE with the lower concentration (relative to the etch products).

The steps just described have been shown to increase the local damage threshold of scratches beyond 30 J/cm^2 . While this appears sufficiently high, additional process optimization was necessary to reduce the probability that no part of a scratch on a large optic damages below NIF-use fluences, including those fluences at the higher end of the fluence distribution shown in Fig. 8. To verify the performance of AMP2 etching on a large optic, we tested a large ensemble of scratches and calculated the damage probability of scratches for a given width per millimeter of scratch length. As shown in Fig. 11(b), the damage probability decreases strongly with etch removal.³⁸ The mass-transport etch model predicts that the wider a scratch opens, the more effective the transport of etch products from the surface will be, which should reduce the probability of precipitation. Also, a wider etched scratch opening is more easily coated with an anti-reflective AR sol-gel -- higher aspect ratio etched scratches leave coating flaws which increase damage probability. The desired removal can be estimated using the data of Fig. 11(b)

along with the scratch length distribution of Fig. 10. Scratches of a given length and width generally have the same number of trailing indent fractures. Therefore, multiplying scratch length (Fig. 10) by indents per scratch and the probability of damage for a given width per unit length (Fig. 11(b)) yields the expected number of damage sites per optic. This calculation predicts less than 10 sites per full-sized optic for a 26 μm etch removal. Figure 12 provides a representative demonstration of how the AMP2 production process affects both scratch morphology and scratch damage density.^{38,43} As shown in Fig. 12, AMP2 trades off increased damage resistance for surface roughness due to etched scratches. While etched scratches can pose a downstream modulation risk, we found that they add only a small increase to the damage probability of downstream optics. This calculation was based on the average number of scratches per optic and the modulation due to an etched scratch of a given width and yielded estimates of less than one modulation-induced downstream damage site per optic. This has been born out empirically: after several years of NIF operation using AMP2 optics, there has been no evidence of modulation induced damage due to etched scratches.

Currently, all fused silica optics in the 3ω section of the NIF laser have been processed with the production AMP2 etch treatment (Fig. 13). After hundreds of high-fluence shots, many at or beyond 1.8 MJ, the number of initiations per fused silica lens has averaged about 10 per installation and none of those damage initiations have occurred on scratches. Work to improve damage resistance continues in order to identify the new set of damage precursors that are expected to become evident at even higher fluences, and to develop whole-optic mitigation techniques for these more-challenging precursors (see AMP3 demo curve⁴⁴⁻⁴⁶ in Fig. 8).

II.A.3. Flaw Management

The optical design constraints of the NIF FOA introduce the risk that, even with damage-resistant AMP2 optics, small imperfections or “flaws” in an optic can perturb the amplitude or phase of the transmitted laser light in such a way as to produce localized intensification on a downstream optic (or surface) at fluence levels sufficient to initiate damage. Optimizing component placement is an important consideration for mitigating non-linear imaging geometries that can exacerbate this effect.⁴⁷ Nonetheless some flaws—for example the sol-gel coating flaw of Fig. 6(b)—are large enough to cause downstream damage regardless of the details of the optical design. Likewise, bulk inclusions and localized finishing anomalies introduced during the optic fabrication process can produce severe intensification at downstream optical planes. Management of these flaws is therefore an important aspect of routine operation of the NIF at high energy and power.

To ensure that optics are not installed with flaws that can lead to downstream damage, each optic is screened to identify the location of potentially-damaging flaws using a system of tools known as FICS (Fig. 6). Each of these flaws is then characterized and assigned a damage threat pass/fail metric, with failing flaws requiring some form of mitigation before the optic can be installed.

In operation, flaws flagged as potentially damaging are typically about 100 μm in diameter, representing $\sim 10^{-8}$ of the full-dimension area of the optic. The small fractional area presents a challenge to the process of documenting and analyzing such features because standard charge-coupled device (CCD) imaging systems that can view the entire optic can only cover each flaw with a resolution of about one pixel. Adequate resolution of potential flaws for a reliable analysis requires an imaging resolution of about 20 pixels per flaw. A two-phased approach is used to meet this challenge. First, a full-aperture image is acquired to identify and locate flaws of

concern. This information is then used to guide the acquisition of high-resolution, sub-aperture data for detailed characterization of the individual flaws.

The full-aperture imaging process targets two types of flaws: those associated with sol-gel anti-reflection coatings, and those associated with surface and bulk anomalies of the fused silica. Both flaw types primarily affect the phase of the transmitted laser light (not the amplitude), and require special lighting and image-acquisition techniques. For coating flaws, the optical surface is illuminated with diffuse fluorescent light and imaged in reflection using a 1024 × 1024 CCD camera located behind an aperture in the light box (Fig. 14(a)). With this design, flaws manifest themselves as deviations in the uniform reflection of the fluorescent light, with flaw information from both optic surfaces being captured in the same image.

For silica bulk and surface anomalies, a backlit dark-field approach is used⁴⁸ in which the optic is translated horizontally while a stationary camera with a linear CCD array acquires vertical strips of data to form a composite image of the optic (Fig. 14(b)). Illumination is provided by a full-height fiber light bar positioned at a fixed lateral offset relative to the CCD array; light from the bar passing through unperturbed regions of the surface (or bulk material) bypasses the CCD, whereas flaws in the surface (or bulk) scatter light into the CCD yielding a bright signal against a dark background.

Flaws exceeding a specified threshold are identified and their positions determined in the coordinate frame of each optic using the image analysis software and referencing methods described in the next section. Once the location of each potential flaw is determined, a more detailed characterization is performed with the PSDI instrument, a custom-built, fiber-based, lens-less version of the PSDI systems developed to characterize the optics and assembled optical systems for extreme UV lithography.^{10, 11} This device collects a series of interferograms that are

used to reconstruct the phase and amplitude perturbations created by the flaw. The phase and amplitude information is input into a customized version¹² of PROP (a fast-Fourier-transform laser propagation code developed at LLNL) that calculates the expected downstream threat posed by each flaw using damage rules described elsewhere.⁴⁹⁻⁵¹ If the probability of downstream damage exceeds a predetermined threshold, the flaw is given a “fail” status and its optic cannot be used in NIF until that flaw is removed or otherwise mitigated (Fig. 15). Coating flaws can be removed with ~95% success rate by stripping and reapplying the AR coating. Surface anomalies can typically be remedied by CO₂ laser repair (Section II.E), while bulk inclusions and other non-repairable flaws can be assigned a spot blocker (Section II.C).

As an example of the magnitude of the flaw management operation for NIF, we currently flag and characterize ~80,000 flaws per year with the FICS systems (not including damage sites), of which about 4% obtain a “fail” damage-threat metric. Of these failures, 9% are non-repairable and require a spot blocker for installation. The FICS stations process ~1800 optics per year (new and recycled), so on average there are about 40 flaws per optic, one or two of which need mitigation. About one in ten optics will have a site that can’t be mitigated by our current methods; in such cases the optic is still useable provided the site is assigned a spot blocker.

II.B. In-situ Damage Inspection and Monitoring

The damage state of the final optics is assessed during operation with the FODI system. The FODI instrument (Fig. 16) is an f/4 600-mm focal length custom optical telescope with 4k × 4k 14-bit cooled scientific-grade CCD camera that can be inserted at target chamber center (TCC) after a laser shot.⁵²⁻⁵³ The telescope and camera ride on a three stage actuation system that slews in azimuth (yaw), elevation (pitch) and hemisphere (roll) to enable accurate and repeatable pointing to each of the 192 beamlines. Fine positioning and attitude of the complete opto-

mechanical assembly is established in the TCC coordinate frame with a hexapod mounted on the end of the positioner boom. The alignment resolution for the system is $\sim 30 \mu\text{m}$ in placement and $20 \mu\text{rad}$ in pointing.

The FODI system is fully automated: pointing, optic illumination and image acquisition are all controlled by the NIF integrated computer control system. A list of beamlines and optic surfaces to be inspected is provided to the instrument control software, and once the instrument is initialized, it can be left to collect the required images with minimal human interaction. A single 192-beam inspection typically inspects 960 optic surfaces and takes 4 hours to complete. At the time of this writing, the equivalent of over 50,000 beamline inspections have been completed with the FODI system, totaling over 230,000 optic surfaces.

The size of a FODI camera pixel scaled to a final optic is approximately $110 \mu\text{m}$, thus FODI cannot spatially resolve damage sites of diameter less than $\sim 300 \mu\text{m}$. Instead, FODI relies on radiometry, using the integrated signal captured from small sites to calculate their area and size down to $\sim 20 \mu\text{m}$ (Fig. 17(a)). Successful use of radiometry requires calibration and a high-quality illumination source. Calibration is accomplished by installing a “truth” optic at representative optic positions. A “truth” optic has a range of known and measured damage sites that can be imaged by FODI and used for calibration. A calibration equation is generated from this data for each optic type and is used by the analysis software to convert the total integrated signal from a site into an estimated diameter.

Stable illumination is provided by a single 30-watt 803-nm laser diode source. The diode light is distributed to the IOMs and individual final optic LRUs by a fiber optic network with a 1:N fiber-optic switch; the computer-controlled switch synchronizes the illumination sequence to the inspection sequence. Compact optical hardware in the IOMs and in each LRU transport and

inject the light into the edge of the optic at angles that cause it to become trapped by total internal reflection. A damage site on the surface of the optic disrupts the total internal reflection and causes light to scatter from that location, a percentage of which is collected and imaged by FODI. In the FODI image of the optic, the damage appears as a bright spot against a dark background with typically high signal to noise (Fig. 17(b)).

A frame of reference for the inspection data is established by applying fiducials to new optics when they are first received from the vendor. The fiducial patterns are made up of groupings of small dots placed around the perimeter of the optic clear aperture using a precision automated translation stage and a focused 10.6 μm wavelength CO₂ laser (Fig. 18). Pattern placement is such that the dots lie outside the region of the optic illuminated by the NIF laser but are still clearly visible with FODI. Dot patterns are unique to each optic type and lack rotation or inversion symmetry to make discerning orientation unambiguous.

The FODI camera system sends acquired images to a computer cluster that performs an automated custom analysis.⁵²⁻⁵⁴ The software analyzes each image to:

1. Detect and measure potential damage sites and assign unique names;
2. Find fiducials and determine the mapping between the image and the optic;
3. Transform site coordinates using mapping from Step 2 to the physical optic coordinates;
4. Categorize defect types and eliminate false alarms;
5. Archive results in a database from which other software applications can pull data for further analysis and reporting.

Step 1 requires finding sites and measuring them accurately using methods that are robust with respect to the relative brightness of the sites and surrounding background. This step requires a custom segmentation algorithm⁵⁵ based on the local signal-to-noise ratio at each pixel in the

image. Finding sites and determining their extent in a consistent and comparable manner allows accurate application of the calibration equations to convert the total intensity for each site into a physical diameter measurement. Figure 19(a) shows a typical FODI image with damage sites identified using the custom segmentation algorithm.

The next two steps (2–3) determine the damage site locations in the optic coordinate frame to within ± 0.5 mm so that individual sites can be uniquely identified and monitored on future inspections. Monitoring provides the site-by-site information about size and rate of growth that is important for projecting spot blocker demand and optic exchanges. Figure 19(b) shows an example of a site that was identified and monitored over a period of time that included the removal of the optic and its re-installation on a different beamline. This site subsequently became active (started to grow), and eventually reached the maximum size that can be mitigated with confidence, at which point it was assigned a spot blocker.⁵⁶

Step 4 applies machine learning for site classification. A detectable feature in an inspection image can fall into one of several categories, such as damage site, reflection of a damage site, reflection of hardware, or damaged CCD pixels (caused by radiation for example). Ruling out irrelevant sites is as important as finding actionable sites to ensure that the system is not flooded with false positives and rendered ineffective. We employ the Avatar suite of machine-learning tools⁵⁷⁻⁵⁹ to “learn” the difference between these categories and determine the most probable classification for new sites.

Finally, Step 5 stores the data in a database where it can be used by custom visualization tools to support optics performance assessment and decision-making.⁶⁰ For example; the Blocker Advisor tool assists operators with making the decision of when to block a growing damage site (Fig. 20). It displays sites that have been classified as damage by the Avatar machine learning

tool, and that have been classified as growing by the optics inspection algorithms. Various filters can be applied by the operator to reduce the number of damage sites displayed, for example by showing only sites over a specified size. Inspection schedules are such that on the order of 10 to 20 sites are presented for consideration by the Blocker Advisor per inspection. Once these recommendations are verified and submitted, the application of the specified spot blockers proceeds automatically.

For this process to be effective, it is important that the rate of false negatives be kept very low, and for damage approaching sizes that require blocking, the probability of failing to detect approaches zero. False positives must also be minimized because in addition to degrading efficiency, they use valuable spot blocker capacity on sites that don't require blocking. Currently, the false positive rate for sites classified as actionable—i.e. requiring a spot blocker or mitigation—is less than 2% after Blocker Advisor review. False negatives are very rare, occurring at a rate of less than 0.05%.

II.C. The Programmable Spatial Shapers

The ability to temporarily shadow a small number of growing damage sites on each final optic from the incident laser fluence provides NIF with a high degree of flexibility for scheduling downtime for optics removal and replacement. NIF has one programmable spatial shaper for each quad—that is, 48 PSS units for all of NIF. Each PSS can produce small shadows in the pattern of 3ω light at threatened sites in the FOA by creating precision obscurations, or “spot blockers,” at a plane just after the regenerative amplifier where the beam is still small and has low energy and power. The specific x, y location for spot blocker placement is informed by the FODI system analysis of the threatened site. The closely coupled FODI and PSS systems form the second innermost loop of the optics recycle loop that enables uninterrupted use of the facility

at near-peak laser performance until optics can be conveniently scheduled for recycling, refinishing, or replacement.

The PSS units that create the spot blockers for each quad are installed at a system relay plane (called relay plane zero, or RP0) in the pre-amplifier module (PAM) upstream of the main amplifier. As illustrated in Fig. 21, at this location the beam is 1/20th of its final size, enabling the use of a practically sized shaper. NIF's relay imaging architecture ensures that features imprinted on the beam at this location are faithfully scaled to the FOA.

The NIF PSS design meets a demanding set of requirements through the use of optically addressable light valve (OALV) technology^{61, 62} that eliminates many undesirable artifacts associated with pixelated modulation of coherent beams. The design of the device and its detailed operation have been described previously^{63, 64} and are briefly reviewed here. Each PSS device has two stages of liquid-crystal-based modulators. In the first stage, an address image is created using a pixelated liquid crystal on silicon (LCoS) modulator, such as is used on many commercial display projectors. The LCoS writes a desired bitmapped profile onto an incoherent 470-nm LED source, which is then projected onto the second-stage OALV. The OALV consists of a large, single-pixel twisted nematic liquid crystal cell in series with a layer of photoconductive bismuth silicon oxide. These layers are surrounded by transparent indium tin oxide (ITO) conductive coatings. While the cell is biased with a common voltage applied to the ITO coatings across its entire aperture, the photoconductive layer enables the intensity of the (above band gap) address beam to locally control the voltage supplied to the liquid crystal layer. The address image pattern thus modulates the polarization of the coherent beam at 1053 nm, and a downstream polarizer enables the polarization modulation to be manifested as an amplitude

modulation. The bitmap profile can then be written onto the coherent beam in a manner that naturally yields smooth apodized patterns free from spurious pixelization artifacts.

OALVs as large as 24 mm × 36 mm were custom designed and fabricated for NIF with low wave-front distortion and anti-reflection coatings, enabling both high transmission and etalon suppression to avoid spectral and temporal ripple. The clear aperture of the OALV accommodates a front-end square-beam profile (18 mm × 18 mm). This technique can produce spot blockers that have smooth shapes, high transmission (>90%), and low wave-front distortion (<0.5 waves) with no spectral distortions.

Spot blocker diameters and edge profiles were carefully chosen as a tradeoff between maintaining usable beam area and minimizing diffraction ripples at edges, which could be intensified and lead to downstream optical damage. Laser propagation studies suggest that the spot blockers can be only as small as 1 mm at the OALV (2 cm on the magnified beam downstream) before Kerr nonlinear effects coupled with edge diffraction introduce significant modulation on the beam, particularly at the second lens (SF4) of the transport spatial filter.⁶⁵

The PSS system was commissioned in 2010 and forms an integral part of the loop strategy. Its ability to introduce programmable spot blockers before the next shot provides flexibility for NIF operations to schedule optic transactions at opportune times. Programmable spatial shapers are in regular use in NIF, helping to keep the shot rate as high as possible and thus the data rate produced for NIF users as high as possible. Figure 22 shows measured high-energy beam profiles as influenced by the 48 sets of PSS patterns in use on June 8, 2012.

The ability of the OALV hardware to arbitrarily pattern a NIF beam profile offers future enhanced performance for the laser. A sophisticated control system that can be used to arbitrarily

sculpt the NIF beams to provide a flatter fluence profile at the FOA is currently under development. Plans are also under consideration to develop and implement a system of 192 shapers for patterning each individual beam instead of each individual quad.

II.D. Damaged Optic Removal and Replacement

An integrated mechanical system enables the rapid, efficient removal and replacement of damaged optics. Each ready-to-install replacement optic is assembled into a lightweight highly-portable frame structure to construct an LRU. The LRUs interface with IOMs within each FOA, as shown in Fig. 4. IOMs are only rarely removed from the target chamber; they are precision-aligned prior to installation, including some adjustments that are beamline dependent. The optic LRUs, on the other hand, must facilitate frequent exchanges while ensuring that alignment requirements continue to be met. Requirements for the LRU structures include:

- accurate positioning of the optic inside the IOM;
- support of high-throughput assembly and optic exchange;
- lightweight, yet with adequate handling features; and
- space and support for edge illumination optics to be used for in-situ damage inspection.

LRUs are supported inside the IOMs using a precision kinematic mounting system. The system allows LRUs to be installed with a tip-and-tilt repeatability of better than 50 μ rad with no adjustments required following installation. This level of accuracy enables rapid exchanges without extensive realignment and re-commissioning.

In addition, LRUs require minimal assembly time. Their reusable frames are fabricated to a level of precision that accommodates the tightest alignment requirements (primarily tip/tilt) of

the LRU, leaving only the relatively loose alignment requirements to be adjusted during assembly. For example, the 250- μ rad tip/tilt accuracy required on some LRUs is achieved using features that are permanently machined into the frames. It would otherwise be necessary to align the kinematic interfaces with respect to the optic with an accuracy of ~ 0.05 mm along the optic axis in order to achieve this requirement. If the kinematic alignment were performed during assembly for each recycled optic, the assembly time would increase, and far more complicated alignment and metrology tooling would be required. With the approach we have taken, the only alignment task performed during assembly for the GDS and WFL LRUs is the x/y centering and rotation about the z axis (the beam propagation direction). The assembly technician must position three datum points on the optic to within ~ 0.5 mm, which can be achieved quickly and easily while installing the optic into the frame.

The final optic LRUs are lightweight to allow safe handling in the difficult working conditions of the NIF target bay. The LRU frame hardware typically accounts for only 10–20% of the total fused silica LRU mass. Handling rails allow LRUs to be lifted safely and help guide the units as they are transferred between different cases and processing tools.

The system of tools for LRU handling has played an important role for the safety and efficiency of loop operation. The central piece of tooling, the loop case, is used for multiple steps within the loop, including IOM LRU exchange (Fig. 5), transportation, environmentally controlled storage, transfer into inspection areas, and transfer into damage mitigation machines. After an LRU is assembled, it is loaded into a loop case, which will protect it for the remainder of its journey throughout the recycle loop. More than 325 cases are currently circulating throughout the loop. The cases are lightweight (< 25 lb. empty) and can safely transport and handle an LRU in any orientation. A standardized case structure is configurable for five of the

six LRUs downstream of the target chamber vacuum window. The GDS LRU uses a special smaller case, which is conceptually identical and shares many common parts with the larger loop case. When an LRU is exchanged, the loop case is docked directly onto the IOM using an LRU-specific adapter flange. The adapter flange is installed in place of an IOM access door and aligns the case to the correct slot in the IOM. The installation process, which is fairly straightforward, takes ~30 min and involves the following steps:

1. Remove the appropriate IOM door.
2. Install the LRU-specific adapter flange.
3. Dock the loop case onto the adapter flange.
4. Drive the LRU into the IOM slot using externally actuated drive wheels.
5. Remove the loop case.
6. Engage the LRU latch (which docks the LRU into the IOM kinematic mounts).
7. Remove the adapter flange.
8. Replace the door.

For LRU removal, the process is reversed. Using only a small set of adapter flanges, an installation team can install any final optics LRU on NIF.

The processes just described protect both the IOM and the final optic LRU from exposure to the ambient environment except for the very short time required to remove the adapter flange and replace the IOM door. This approach is consistent with the rapid exchange philosophy developed in 2000–2001 for assembling the entire NIF optics exoskeleton infrastructure. The approach allows repeated removal and replacement of final optics while maintaining their cleanliness by minimizing their exposure to target bay air. Because of the large number of simultaneous work activities required in the target bay, air conditions can get up to ISO 6 (≤ 1000

particles $\geq 0.5 \mu\text{m}$ per ft^3). In locations where the optic LRUs are exposed for longer durations, the ambient environment is maintained at a higher level of cleanliness, ISO 5 (≤ 100 particles $\geq 0.5 \mu\text{m}$ per ft^3).

The same loop cases are used with similar interface tooling to install (and remove) LRUs into (and from) inspection areas and mitigation machines. The LRU and loop case designs are central to the entire mechanical system that enables the efficient exchange and repair of damaged optics.

II.E. Damage Site Repair with CO₂ Laser Ablation

Laser-induced surface damage sites on fused silica optics are repaired using an infrared wavelength CO₂ laser to evaporate or ablate away damaged material and arrest each site's subsequent growth.⁶⁶⁻⁷⁶ This approach benefits from the relative ease with which the laser spot size and power modulation may be varied and the ready availability of industrial-grade CO₂ lasers with sufficient power. The approach differs from others that rely on thermally induced flow, slow evaporation, or a combination of the two. For example, mid-IR lasers ($\sim 4.6 \mu\text{m}$) that absorb in the multi-phonon region of SiO₂ have been used to heal subsurface fractures related to optical damage.^{70, 71} CO₂-laser radiation ($9\text{--}11 \mu\text{m}$) is more effective at achieving the high peak surface temperatures required for evaporation. The strong optical phonon resonance in SiO₂ near $9 \mu\text{m}$ gives rise to an absorption depth at $10.6 \mu\text{m}$ of only a few micrometers.^{77, 78}

A critical requirement for a damage mitigation process, in addition to damage repair⁷⁹ and introduction of low residual stress,^{80, 81} is that intensification of laser light passing through the repaired site must remain below the damage threshold of downstream optical surfaces.⁸² Surface structure resulting from structural relaxation,^{83, 84} thermo-capillary flow,⁸⁵ and

evaporation⁸⁶ can lead to such intensification. These mechanisms often produce a raised rim surrounding the evaporation pit that can be several micrometers high, depending on temperature, the duration of the laser treatment, and the volume of material melted. Light refracted from the outer edges of this rim can form an intense downstream focused spot capable of damaging fused silica optics.⁸² The propensity for thermo-capillary action (and therefore downstream modulation) can be characterized by a modified or transient form of the well-known Marangoni number, $M_a' = \sigma_M/\sigma_V$, where σ_M and σ_V are shear stresses associated with the Marangoni effect and viscosity, respectively. In our analysis, σ_M is proportional to the surface-temperature gradient times the derivative of the surface tension as a function of temperature, while σ_V is simply the viscosity divided by the exposure time. Figure 23(a) shows M_a' as a function of temperature for short, moderate, and long pulses. Generally, as temperature increases (and surface tension gradients become stronger), material tends to flow more readily, producing rims capable of focusing light that would endanger downstream optics. Reducing M_a' to near or below 1 sufficiently minimizes rim height.

The NIF CO₂ laser mitigation technique manages these trends by using a tightly focused 10.6- μm laser spot ($\sim 100 \mu\text{m}$), high irradiance ($\sim 1 \text{ MW}/\text{cm}^2$), and a short pulse ($\sim 10 \mu\text{s}$) to minimize the volume of material melted and the duration of melting.⁷³ Figure 23(b) compares this operating regime with other published approaches. For $T > 4000 \text{ K}$, pits evaporated by a single pulse are $\sim 40 \mu\text{m}$ in diameter and a few micrometers deep. Due to the short laser deposition time and therefore limited M_a' values, the mitigated damage site rim height is $\sim 100 \text{ nm}$ instead of several micrometers. Laser damage sites with dimensions up to $500 \mu\text{m}$ wide and $300 \mu\text{m}$ deep can be mitigated and prevented from growing upon re-irradiation. Galvanometer-driven steering mirrors repeatedly scan the CO₂ laser spot over the damage site.

The scan pattern, a series of circles with varying radii, is designed to create a conical pit (Fig. 24). The rim surrounding the final pit can be kept small, at ~ 100 nm, because the time between pulses allows adequate cooling. The technique described here was chosen over several others we investigated, because the final dimensions and shape of the cone are almost completely independent of the initial damage morphology, making the process largely deterministic and predictable. By controlling the scan pattern and pulse energy, we can produce cones that “match” the dimensions of the damage and produce both straight and parabolic cone wall shapes that offer even finer control of downstream intensification. The small volume of material melted per pulse and the short duration allowed for material response leave comparatively low residual stress. The amount of evaporated material re-deposited on the optical surface is also comparatively low because of the high evaporation temperature (3500–4000 K) resulting in a higher velocity of the evaporation plume away from the surface. Finally, although a large number of laser pulses are used ($\sim 10^6$) per mitigation, they are applied in rapid succession, keeping the total mitigation time commensurate with other optic processing steps (on the order of minutes; see Table I).

Interestingly, few other groups developing damage mitigation strategies have explored this temporal-irradiance portion of the laser-processing map (Fig. 23(b)). Those approaches may still be successful because the downstream modulation requirements for the other systems may be less stringent than they are for NIF (the positioning of downstream optics directly impacts those morphologies which are acceptable) and because the operational demand at NIF helped focus efforts that led to our approach.

LLNL’s OMF, a production facility built to deploy these techniques, houses four semi-automated laser repair stations. After an optic in its LRU is loaded onto a large two-axis

translational stage, the optical surface is located to within 20 μm with a noncontact chromatic confocal sensor, and the optic lateral coordinates are computed after registration of fiducials (see Fig. 7). An operator inspects and photographs each site on the damage list provided by FODI (Section II.B) as well as any surface flaws identified by FICS as requiring mitigation (Section II.A.3) and assigns a repair protocol. Various protocols are available, depending on the size of the damage site (Table I). The system then executes repair protocols at all locations flagged for repair. Post-repair images are obtained as part of our quality assurance effort.

III. OPTICS RECYCLE LOOP OPERATIONS AND PERFORMANCE

As discussed in Section I, the optics recycle strategy consists of four nested loops: Inspection & Block, Recycle, Refinish, and New optic. Table II compares the cycle time, rate, and approximate relative cost in procurement and labor of each loop. Large savings in cycle time and cost, and significant increases in capacity (rate) are realized by operating in the two inner loops (Inspect & Block, Recycle) and minimizing the two outer loops (Refinish, New optic).

To sustain continuous operation, the supply of 3ω optics to the laser must equal the demand—the rate at which optics exit the Inspect & Block loop and are removed for refurbishment. In general, this demand is a strong function of the experimental shot plan (rate, energy and power), the damage resistance of the optics, and the number of spot blockers allowed per quad (Section IV). For the purposes of this section, it is also the ratio of the spot blocker use rate to the spot blocker capacity:

$$\textit{Optics per shot} = \frac{\textit{Spot blockers added per shot}}{\textit{Spot blocker capacity per optic}}$$

The problem of load-leveling optics demand is thus one of load-leveling spot blocker use. The spot blockers added per shot is largely determined by the damage growth per shot (Section IV);

therefore, spot blocker load-leveling is achieved by establishing and enforcing guidelines for allowable damage growth in the shot plan.

Detailed projection of demand for the planning of optics exchanges is done on the order of one to two weeks in advance by extrapolating the spot blocker state of the laser forward using the expected damage growth rate from the shot plan and the current damage state of the optics from FODI. Figure 25(a) shows an example of one such projection and how it is used to identify candidate optics for exchange that are in danger of driving the spot blocker count above capacity. Sustained application of this process by an ever-vigilant staff keeps the use of the NIF spot blocker resource optimized so that the flow of optics to the Recycle loop can progress according to plan (Fig. 25(b)).

Figure 26(a) shows the trend in cumulative optics throughput and damage site repair since commencement of Recycle loop operations in 2010. Operation reached full capacity in the latter half of 2012 shortly following completion of OMF facilitization, demonstrating the ability to sustain optic exchange rates of ~40 per week in support of routine 1.8 MJ laser operation for the National Ignition Campaign (NIC). By the end of the NIC in fall of 2012, over 1500 optics had passed through the Recycle loop with over 50,000 damage sites repaired. Learning and process improvements had brought the unit cost of optic recycling down to a small fraction of the cost for refinishing or replacement (Fig. 26(b)). Subsequently, the rate of the Recycle loop was adjusted to match NIF shot rate and fluence demands consistent with post-NIC budget constraints.

After several years of operation, the majority of the optics currently installed on NIF have passed through the Recycle loop at least once, with some having been recycled over 8 times (Fig. 27(a)). Individual optics can and have accumulated over 100 repaired sites while maintaining a

total obscuration level well below the current specification of <1% (Fig. 27(b)). Yield of the mitigation process is quite high: currently ~98% of the damage sites inspected in OMF are repairable, and the failure of those repairs is <0.1%. Recycled optics typically reach end of life when they accumulate 3–4 flaws or damage sites that cannot be repaired, either because they are too large, too deep, or too close together. The so-called “permanent” spot blockers that would be required to install and use such an optic constitute such a large fraction of the total spot blocker capacity for a quad that the optic is instead sent on to the next loop to be refinished or replaced. Currently this “fall out” from the Recycle loop occurs at a rate of ~10%. Recalling that recycle rate (and therefore shot rate) is directly proportional to spot blocker capacity; the total number of “permanent” spot blockers in use at any one time must be monitored and actively managed. Currently, ~28% of the total NIF blocker capacity is allocated to protecting 318 sites on 208 optics requiring “permanent” spot blockers, against a budget of 25%. At less than one site per installed recyclable optic, there is little leeway for lowering this budget to regain lost blocker capacity. On the other hand, a 4× increase in spot blocker capacity that could be gained by moving to a beam-based PSS architecture remains a topic of great interest.

IV. IMPLICATIONS FOR LASER OPERATIONAL CAPABILITY

The integrated set of technologies and production processes comprising the NIF optics recycle loop provides an enabling capability that has allowed NIF to operate at—and beyond—its design specifications for 3ω energy on target. To our knowledge, this operational methodology is unique to NIF; it has not been successfully fielded on any other laser system. The impact of the recycle loop on NIF 3ω operational capability has been profound, allowing the experimental program to routinely access 3ω energies that would have otherwise been unachievable.

An important metric for quantifying the operational capability provided by the recycle loop is the shot rate that can be sustained at a specified laser operating point. Laser operating points are often described simply in terms of energy or power, but for the purposes of assessing optical damage and the recycle loop we must also account for the pulse format in which the energy and power is delivered. Summarizing briefly, for any given laser pulse there are two pulse-specific parameters that drive fused silica damage and recycle demand. The first is the 3ω fluence of the pulse in the final optics, straightforwardly estimated from the energy on target:

$$F = E_{TCC} / (N_B \cdot A \cdot T_{3\omega})$$

Here N_B is the number of beams, A is the beam area in the final optics ($\sim 1240 \text{ cm}^2$), and $T_{3\omega}$ is the 3ω transmission to target, including losses in the disposable debris shield (~ 0.9). The 3ω fluence determines the rate at which optical damage initiates (sites per optic per shot) according to the measured damage density versus fluence relationship $\rho(F)$ for the optics (see Fig. 8) and the max-of-N fluence statistics of the laser.⁸⁸ With the wide range of pulse shapes that can be employed on the NIF, we adopt the convention here and elsewhere of specifying the fluence important for initiation of damage on fused silica exit surfaces in terms of its 3-ns Gaussian pulse equivalent:

$$F_{3ns \text{ Equiv}} = F \cdot \left(\frac{3.0}{\tau_{\text{Equiv}}} \right)^{0.5}$$

Here τ_{Equiv} is the duration of a Gaussian pulse that has the same energy as the laser pulse and that produces the same localized defect heating according to the diffusion model of Ref. 14. The 0.5 power of the pulse length scaling has been empirically established for fused silica and is related to the dimensionality of the diffusion mechanism. For reference, the τ_{Equiv} pulse duration of the

1.8 MJ NIF design pulse on which the laser's functional requirements are based is 3 ns. The ignition pulses employed during the NIC and subsequent to the NIC have tended to have shorter τ_{Equiv} durations in the range of 2 to 2.5 ns. Shots with these shorter equivalent pulse lengths are more threatening to the optics even though they deliver the same energy, because damage initiation can occur at fluence levels below those for the 3 ns effective pulse lengths, fluence levels reduced by a factor of 1.22 to 1.1, respectively.

The second parameter is the damage growth factor of the pulse, which determines the rate at which an exposed pre-existing damage site will grow in size^{5,89} and therefore the number of shots that can be taken before a damage site reaches the maximum allowable size for repair and requires a spot blocker. As discussed in the introduction, laser damage on fused silica grows exponentially with fluence:

$$D_{Shot\ n} = D_{Shot\ n-1} e^{\alpha}$$

where the exponent α – also referred to as the ln(Growth) – depends primarily on fluence and to a lesser extent on other details of the laser pulse shape and the site size. Specifically, ln(Growth) is a thresholded function of the total fluence in the pulse, including the residual fluence of the first and second harmonic wavelengths exiting the frequency converter. The function is thresholded in that only the total fluence accumulated after a time $t = t_{thr}$ when the 3ω intensity first exceeds $\sim 0.3\text{ GW/cm}^2$, contributes to the growth process:⁸⁹

$$\alpha = 0.033(F_{Growth} - 4.0\text{ J/cm}^2), \quad F_{Growth} = \sum_{j=1,2,3\omega} \int_{t_{thr}}^{\infty} I_j(t) dt$$

The approximate relationships of α and $F_{3ns\ Equiv}$ to 3ω laser energy and power are shown in Fig. 28, which plots these two parameters for three different ranges of power on target versus

the full-NIF-Equivalent laser energy for all NIF shots between September 2011 and June 2014 (that used 50 or more beams on a shot). The limits of the power ranges are described in the caption of Fig. 28. As these plots demonstrate, low power shots can have higher growth factors than high power shots of the same energy, due primarily to their lower conversion efficiency and higher levels of unconverted light. Conversely, for the set of shots taken up to the present time, high power shots tend to have substantially higher 3-ns equivalent fluences than low power shots of the same energy due to their shorter τ_{Equiv} . For the following analysis we focus on the higher power data set that is most representative of ignition pulses, and that scales approximately with energy as indicated by the trend lines.

Estimation of the shot rate that can be supported by the recycle loop at a specified laser operating point employs a simple steady-state model with the following inputs:

- The approximate energy-dependence of α and $F_{3ns\ Equiv}$ described above
- The $\rho(F)$ of the fused silica optics
- The maximum number of allowed blockers per quad
- The capacity of the recycle loop.

In this model the loop capacity is characterized by two parameters: the steady-state number of optics that can be exchanged per week as limited by scheduling, resources, inventory, etc., and the steady-state number of damage sites that can be processed per week in the NIF mitigation facility, OMF. Here we consider the case directly relevant to NIF operation during NIC, in which the blocker and loop capacities are those demonstrated in the final year of the campaign: 24 blockers per quad (75% of which are available to shadow growing damage, 25% of which are assigned to semi-permanent protection of other vulnerable sites on optics not subject to growth), 40 optics per week exchange rate, and 1000 damage sites per week mitigation rate. The

calculations further assume a damage initiation size of 10 μm , a blocker-necessary size of 300 μm and a threshold size for repair of ≥ 50 μm once an optic has reached the OMF.

Figure 29 summarizes the analysis of loop operation, plotted as steady-state shot rate versus 3ω laser energy on target. Two curves are shown for comparison, one calculated for optics with 2007-era surface damage characteristics, and one for AMP2-quality optics implemented during the NIC. With 2007-era optics, recycling is required above 600 to 650 kJ. At this point approximately one damage site per optic is expected at ~ 3 J/cm^2 (see Fig. 8), and the fluence (accounting for all wavelengths) begins to exceed the threshold for damage growth. Operating the recycle loop with these optics is able to increase the operating energy to ~ 1 MJ, but it is insufficient, without more damage-initiation resistant optics, to support operation at 1.8 MJ, a conclusion that remains unchanged even if the loop capacity were doubled (the sustainable shot rate is directly proportional to the loop capacity). In contrast, operating the recycle loop with AMP2-quality optics extends the energy capability of the laser significantly. In this case the increased damage-resistance of the AMP2 optics and the availability of spot blockers pushes the threshold for optic recycling to over 1 MJ. Shots up to ~ 1.4 MJ are supported at rates exceeding several hundred per year, and at the upper end of the operating range, a 1.8 MJ 500 TW NIC ignition pulse is supported at the rate of ~ 60 shots per year. The benefit of operating the recycle loop with damage-resistant fused silica optics is thus clear. With 2007-era optics and no recycle loop, NIF operations would be limited to < 650 kJ. With AMP2 optics and the recycle loop as implemented during the NIC, operation is supported up to 1.8 MJ, an increase in the energy delivery capability of well over a factor of two, approaching an increase of nearly a factor of three.

The simulations described above consider the idealized case of steady-state laser operation at a given laser operating point. In practice, to support its missions, the NIF laser must deliver a variety of pulses over a range of fluences and growth factors. To date, “load leveling” of the optic recycle loop under these conditions has been accomplished by setting guidelines for the rate of damage growth produced by the shot plan, specifically the cumulative $\ln(\text{growth})$ per week. At the time of this writing, the majority of recyclable optics on NIF has passed through the recycle loop at least once (Fig. 27(b)). This fact, combined with periodic high-fluence initiating shots, leads to loop operating conditions in which, upon re-installation, the recycled optics contain the number of small un-mitigated damage sites that is sufficient to fill the blocker capacity. The number of shots an optic can then experience before it must be recycled is therefore the number of shots required to grow the pre-existing sites to blockable size. While only an approximate relationship, the $\ln(\text{growth})$ per week metric has proven to be an effective means of managing the optics recycle rate. Figure 30 plots cumulative recycles versus the cumulative $\ln(\text{growth})$ for the last several years of loop operation. Since the beginning of 2013, the gradient of this plot has remained fairly constant at 115 exchanges per $\ln(\text{growth})$, or about 34.5 exchanges for 0.3 $\ln(\text{growth})$, the current weekly planning guideline for NIF. During this period, the laser successfully delivered 86 shots in the range of 1 to 1.9 MJ for the NIF user community.

V. CONCLUSION

As discussed in the previous sections of this paper, the essential elements of the loop strategy are (1) using optics that are damage resistant and developing the ability to (2) identify the location on an optic that has been damaged, (3) block incident light on a damaged region of an optic, (4) rapidly exchange damaged optics with replacement optics and (5) repair a damaged

optic. At LLNL, we have implemented robust infrastructure and processes for inspecting, blocking, exchanging, and repairing NIF 3ω optics, and we have accumulated over three years of loop operations experience. Improvements in processes and efficiency remain areas of continuing focus; however, the highest leverage for increasing the operational capability of the laser continues to be the damage resistance of the 3ω optics. LLNL has made major advances in this field over the past two decades, and we are continuing to aggressively pursue the next-generation in optics damage resistance.⁴⁴⁻⁴⁶

There are a number of different types of optical damage that can limit the operating point of a laser. With the high level of beam quality that has been achieved on NIF beamlines, and for the range of optical pulse shapes and energies per beam that are requested for NIF shots, exit surface damage initiation on fused silica and growth of these sites are by far that most limiting. The Optics Recycle Loop was designed to raise the operational limit imposed by these two characteristics of fused silica optical damage. Nonetheless, there is still more room for improvement in the NIF operating point before encroaching into limits placed by other types of damage, such as initiation and growth of sites on the exit surfaces of the tripler, filamentation in fused silica optics in either the 1ω or the 3ω regions of the laser, and damage to mirror surfaces in the 1ω region. As work continues for improving the performance of NIF by improving the capabilities of some of the loop subsystems, these other limits are being monitored.

Spot blocker technology is another high-leverage component of the loop. Calculations show that increasing the number of spot blockers available per beam by moving from a quad-based system to a beam-based system has the potential to double the sustainable $\ln(\text{growth})$ per week at current operating costs. Continued development of these important loop capabilities provides the option to increase shot rate at current operating levels, extend NIF operations to

higher energies, or continue to operate at current levels for lower cost. In this way, the loop provides for continuous optimization of the NIF resource in pursuit of its missions.

TABLE I. Various CO₂ protocols used to repair damage sites of various sizes on the input or output surfaces of 3ω fused silica optics in the OMF (after Ref. 87).

Protocol Name	Protocol Diameter (μm)	Maximum Damage Site Size (μm)	Optic Surface	Time to repair (min:sec)	Example image of site to be repaired (500 μm full scale)
RAM2000	2000	800	Exit	5:00	
RAM1260	1260	350	Exit	1:18	
RAM520	520	150	Exit	0:15	
RAM360	360	180	Input	0:51	
RAM600	600	320	Input	0:22	

TABLE II. Rates, cycle times, and relative costs of various loops in the optics recycle strategy during the latter half of 2012.

Loop Cycle	Rate (#/month)	Approx. Cycle Time	Relative Cost (%)
Inspection & Block	~12 times	hours	0.1
Recycle	150	3 weeks	10
Refinish	15	6 months	65
New Optic	10	1 year	100

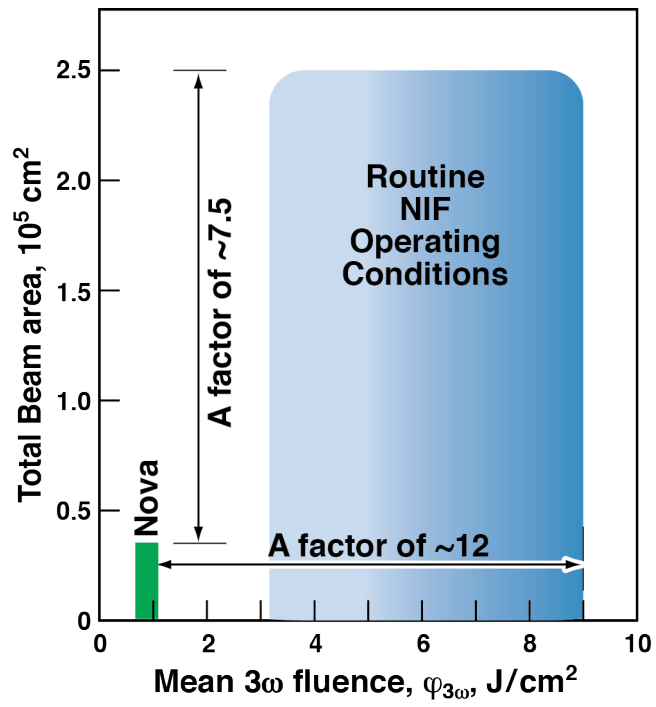


Fig. 1. Comparison of the fluence and beam area requirements for LLNL's Nova laser and NIF.

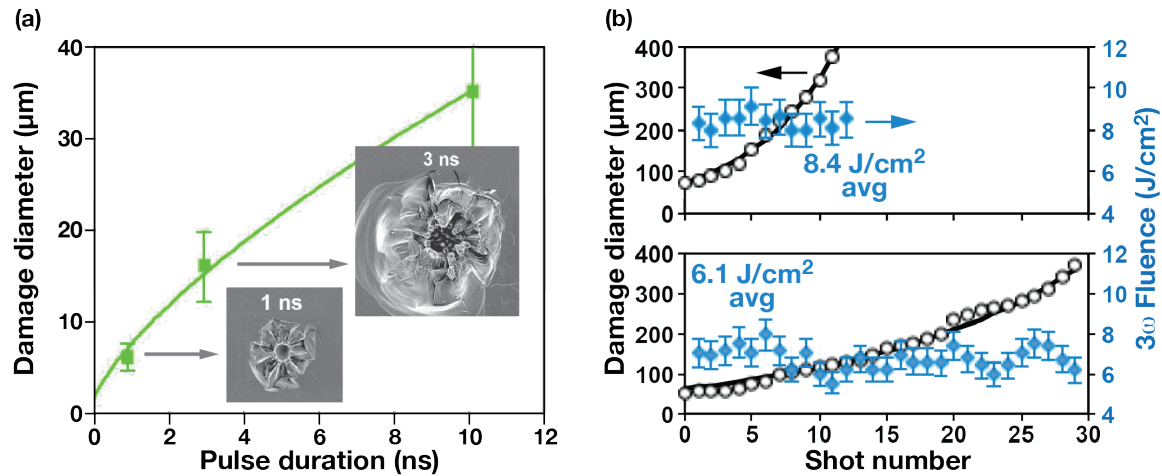


Fig. 2. (a) At NIF fluences and pulse shapes, absorption of sub-band-gap light by damage precursors on an optic's surface can initiate optical damage. Initial damage sites are small, ranging in size from ~ 5 to ~ 30 μm in diameter, depending on pulse length (after Ref. 4). (b) Sub-band-gap absorption on crack surfaces surrounding a site leads to damage growth. The rate of growth is fluence-dependent, and this damage will ultimately limit the optic's service life (after Ref. 5).

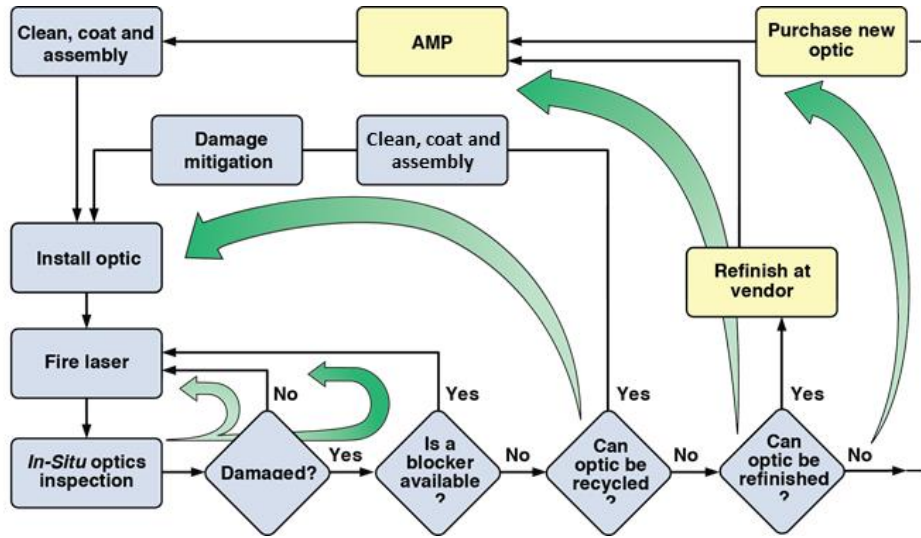


Fig. 3. Optics recycle loop strategy deployed for NIF. Blue rectangles indicate steps required for routine operation of the laser, blue diamonds are decision points related to damage, and yellow rectangles are steps associated with fabricating damage resistant optics.

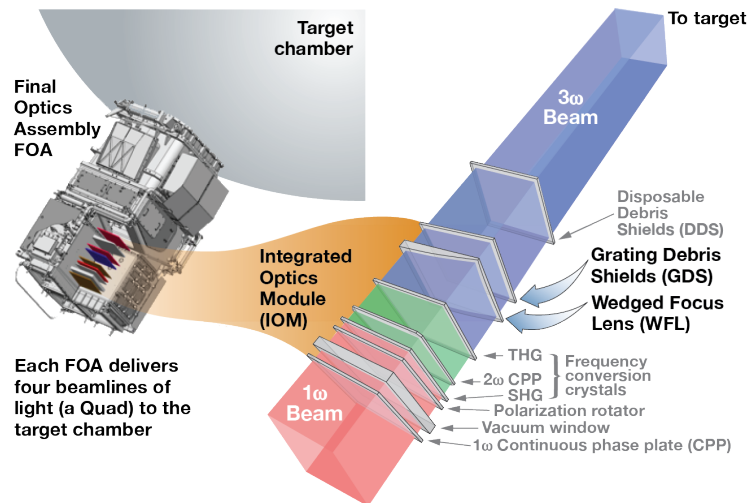


Fig. 4. The NIF final optics assembly (FOA) frequency converts the infrared (1ω) beams from the laser amplifier to the ultraviolet (3ω) and focuses it onto the target. Each FOA handles four beamlines in a 2×2 quad arrangement. The fused silica optics in the FOA 3ω section are at greatest risk for optical damage: the wedged focus lens (WFL) and grating debris shield (GDS). The disposable debris shield located downstream of the GDS is made from inexpensive float glass and is discarded once it becomes disruptively coated with target debris.

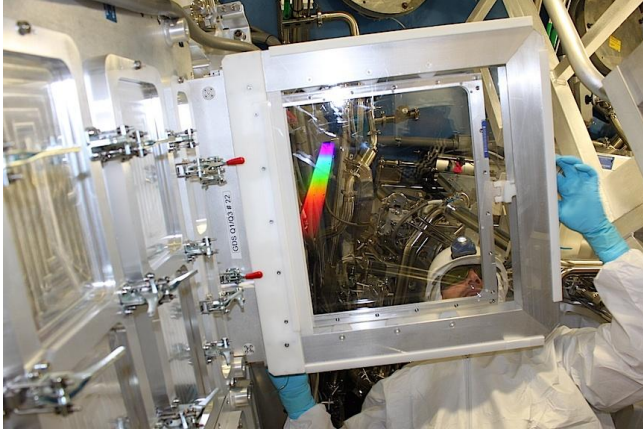


Fig. 5. Clean transfer of a line replaceable unit from the FOA to a loop case in preparation for recycling. Transparent covers on the loop case allow visual monitoring of the transfer.

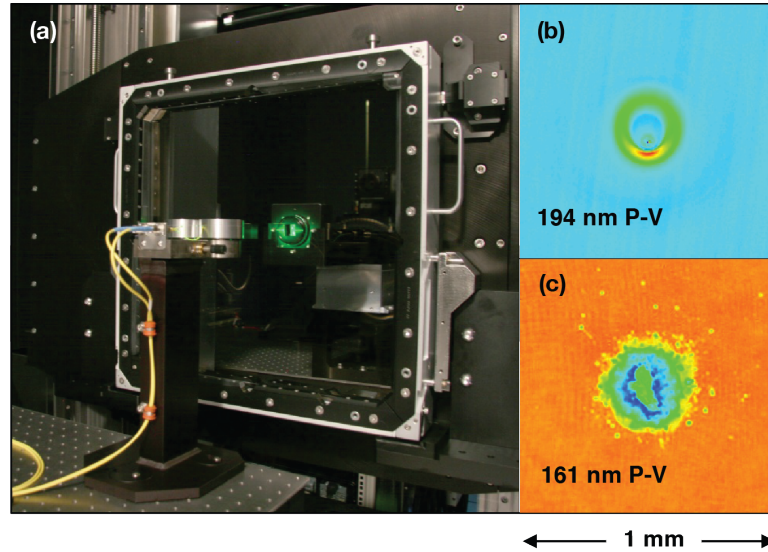


Fig. 6. (a) The FICS locates and measures sub-millimeter-scale optical flaws that would modify the transmitted phase of the high-power laser pulse and cause damaging downstream intensification. Two examples are shown at right: (b) a coating flaw that will be removed with the FLRT system; and (c) a shallow damage site that is stable with respect to growth, but needs repair in the optics mitigation facility before it can be reinstalled without a protective spot blocker. P-V refers to peak-to-valley optical path difference.

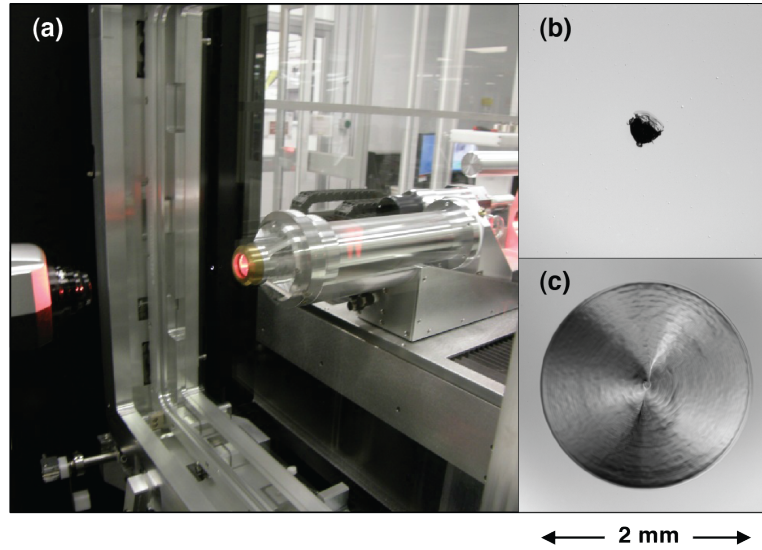


Fig. 7. (a) An optic undergoing repair in the OMF. At right, a typical 3ω damage site as seen with a process monitoring camera (b) before and (c) after repair. During the repair, local temperatures exceed several thousand Kelvin, causing the emission of visible light seen just left of center in (a).

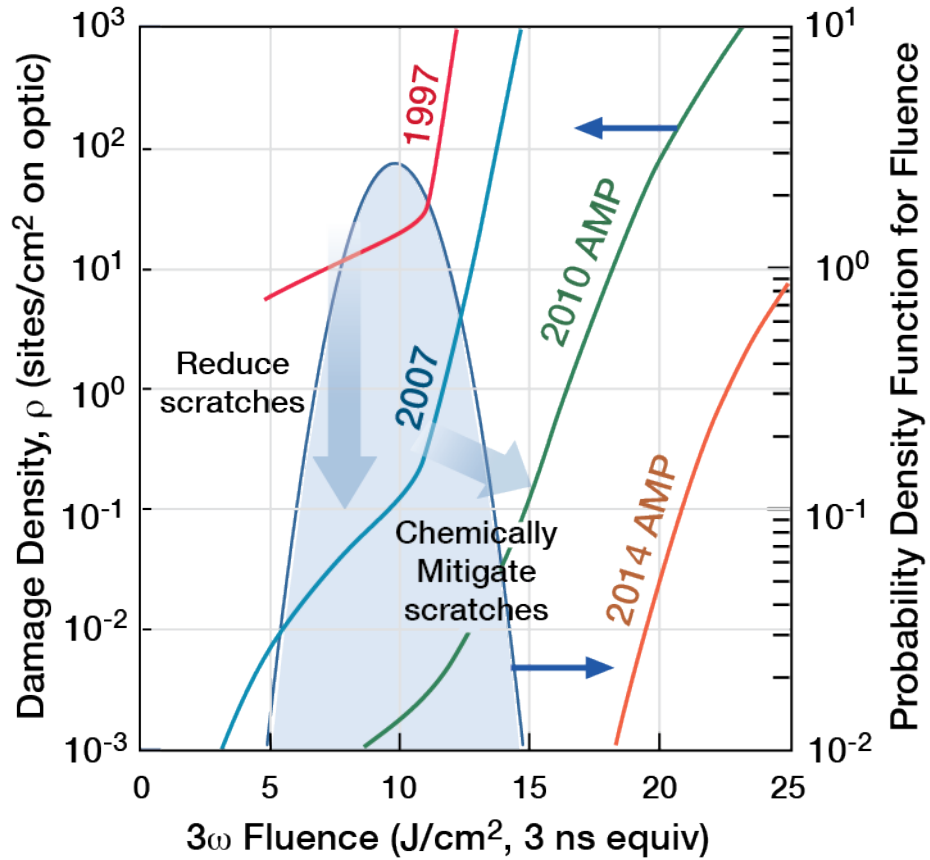


Fig. 8. Laser damage density on a fused silica optic surface as a function of 3ω laser fluence. The lines represent the quality level of the optics at various times, and the shaded blue region indicates the relative fluence distribution expected on a 1.8 MJ NIF laser shot.

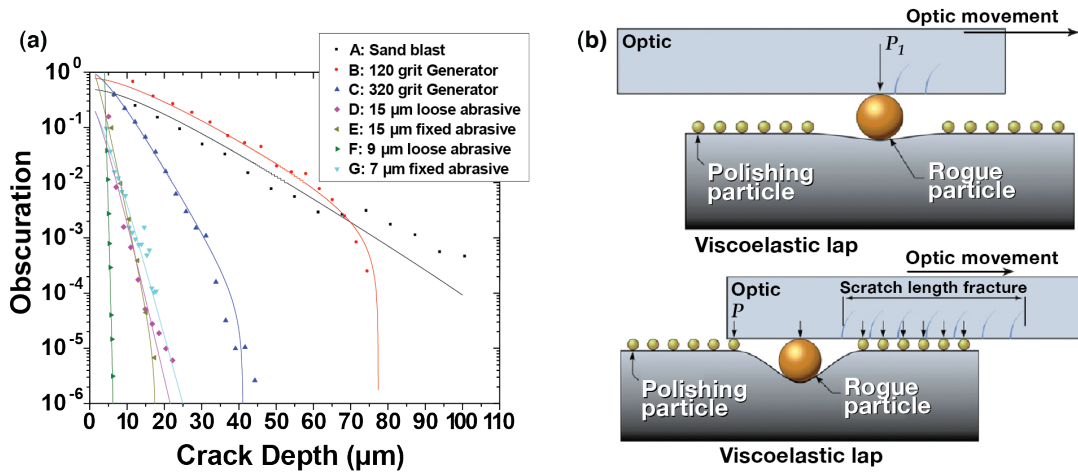


Fig. 9. (a) Statistically measured microfracture depth distributions of various grinding processes; note obscuration is the observed crack area, which is proportional to microfracture number density (from Ref. 19, reprinted by permission). (b) Schematic illustration showing how a scratch is created by a rogue particle during polishing (from Ref. 24, reprinted by permission).

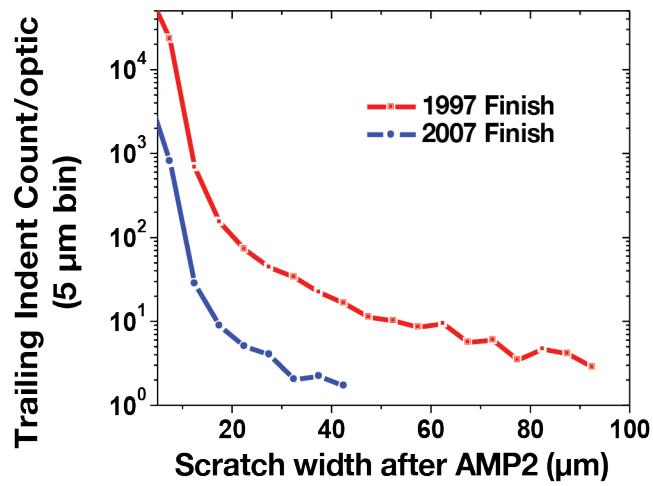


Fig. 10. Scratch width distributions on a typical fused silica optic fabricated with 1997 and 2007 finishing procedures, measured after etching with the AMP2 process. Note the trailing indent count per optic was calculated over 5 μm scratch width bins.

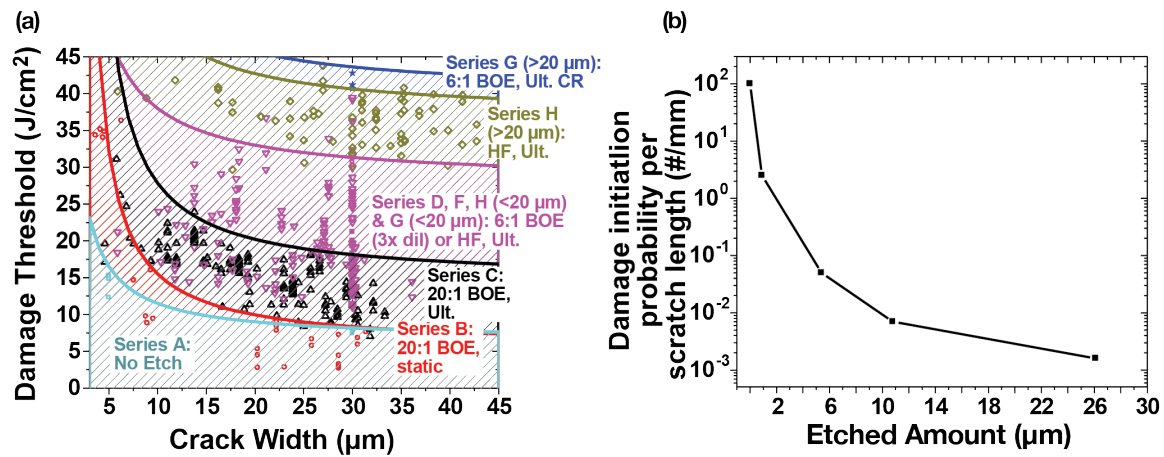


Fig. 11. (a) Results from small-beam laser damage test, where damage is measured as a function of scratch width for various etch processes. The solid lines represent the upper bound of the laser damage threshold for each series. Ult. = ultrasonic or megasonic rinsed; CR = processed in a cleanroom; $<20 \mu\text{m}$ = removal during etch; $>20 \mu\text{m}$ = removal during etch; (b) Probability of large-beam laser damage initiation (351 nm , $12 \text{ J}/\text{cm}^2$) as a function of etched amount for variations in AMP treatment. From Ref. 38, reprinted with permission.

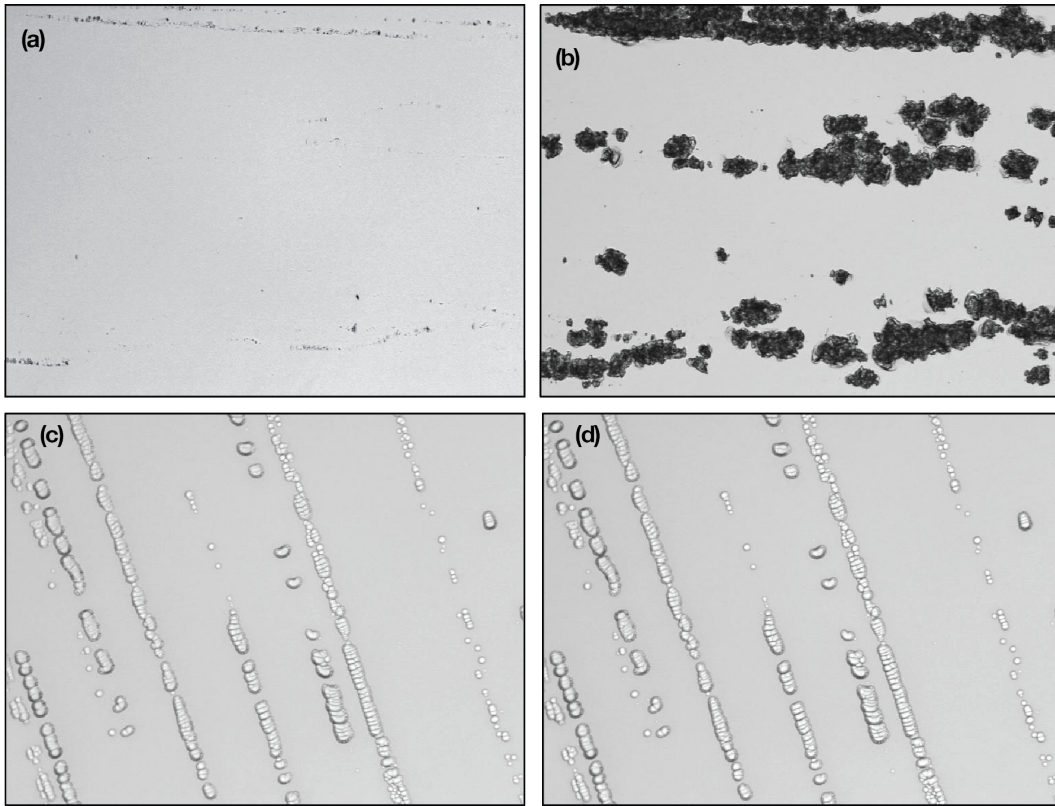


Fig. 12. Optical micrographs of scratches generated on fused silica before (left) and after (right) laser shots at 8, 10, and 12 J/cm² (3-cm beam, 3 ns, 351 nm). (a, b) an untreated, scratched sample and (c, d) a scratched sample after the AMP2 etch treatment. From Ref. 38, reprinted with permission.



Fig. 13. Production-scale AMP2 process station for chemical treatment of 3ω fused silica optics.

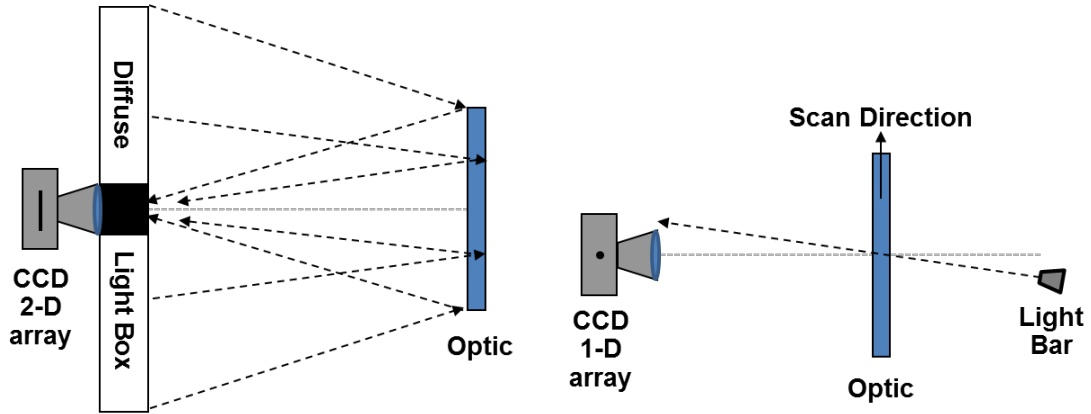


Fig. 14. Full-aperture imaging geometry used to screen optics for flaws in (a) sol-gel coatings and (b) fused silica surfaces and bulk material.

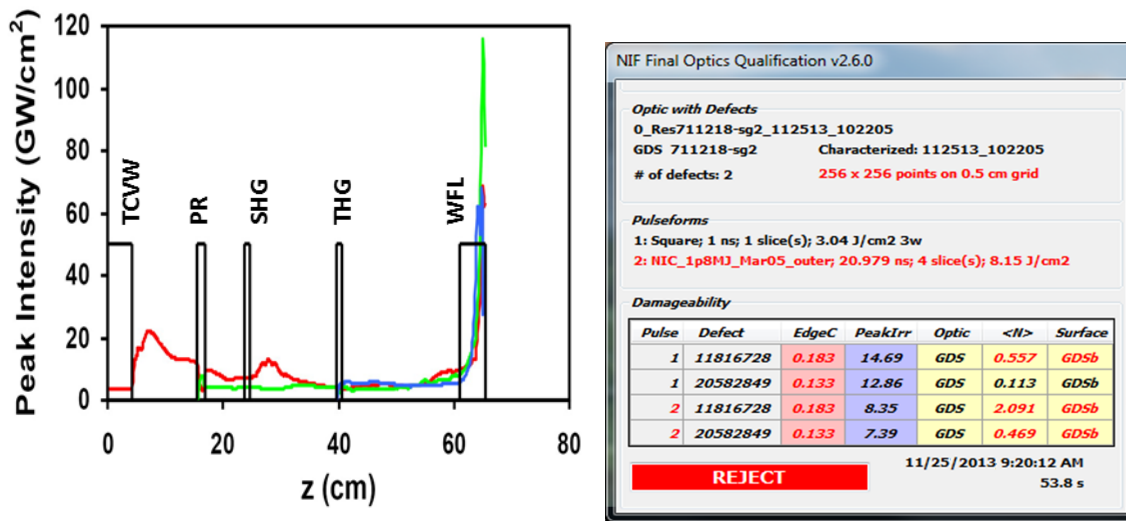


Fig. 15. (a) Graphical output from a FICS damage-threat calculation showing the downstream intensification at 1ω (red), 2ω (green) and 3ω (blue) produced by a flaw on the target chamber vacuum window (TCVW). This flaw would receive a failing damage-threat metric due to the high intensification at the WFL. (b) Example output from the FICS production software summarizing the flaw assessment of a GDS. The flaws are on the GDS input surface and received a failing metric due to high damage expectation values $\langle N \rangle$ at the exit surface.

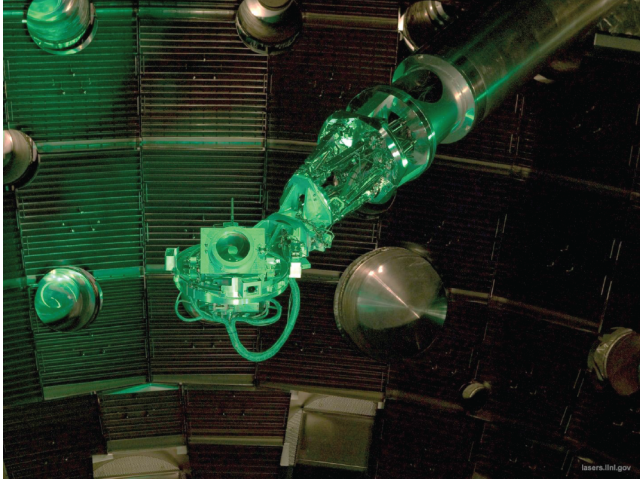


Fig. 16. The FODI instrument is an optical telescope and camera inserted in the center of the target chamber to inspect the optics of each beamline after a laser shot.

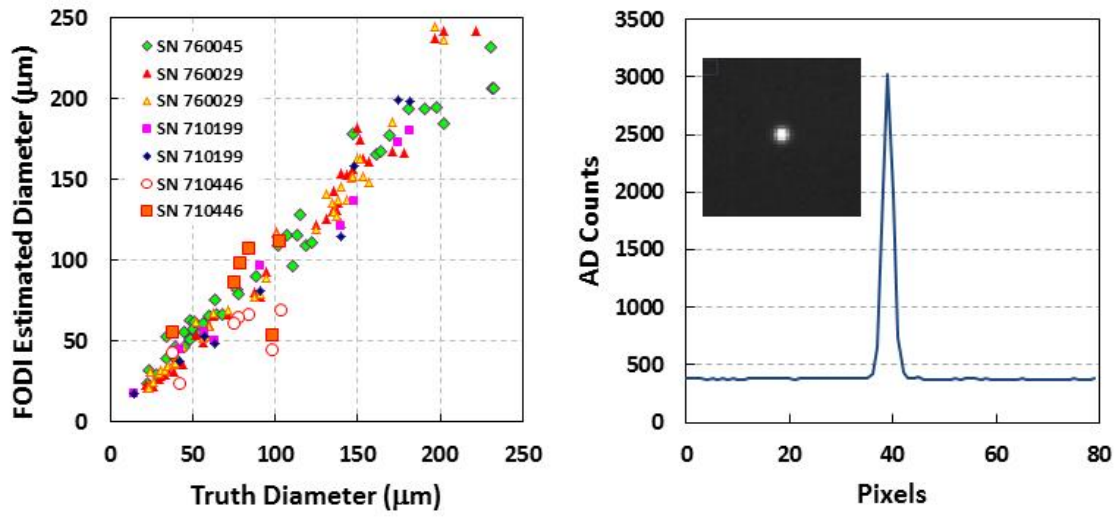


Fig. 17. (a) Plot comparing size measured with FODI to the actual size measured with microscopy of over 200 damage sites on seven different “truth” optics. (b) Representative image data for a 50 μm damage site obtained using ~1W of optic edge illumination at 0.5 sec exposure, demonstrating high contrast between peak signal and background.

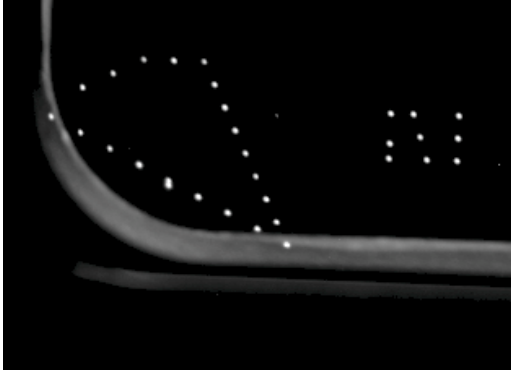


Fig. 18. A cutout from a FODI image showing the fiducial pattern placed in the lower-left corner of a GDS optic. Size of rectangular pattern to the right is 4.5 mm \times 3 mm.

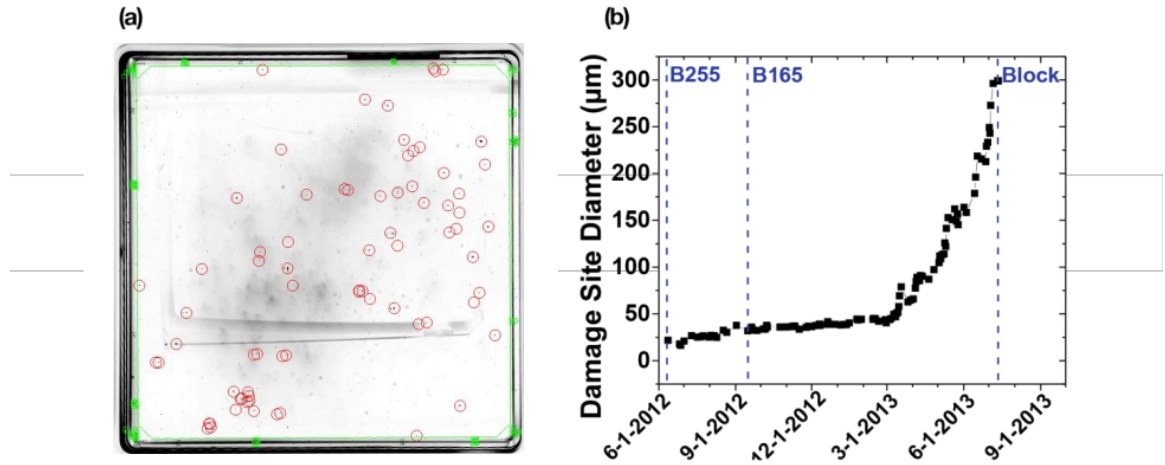


Fig. 19. (a) Example FODI inverted gray-scale image of GDS optic (43 cm × 43 cm) displaying fiducials (green squares) and damage sites (red circles) identified with image analysis; (b) example of a damaged site’s size evolution measured over time using FODI and image analysis. This site evolved and grew on two successive NIF beamlines and eventually was blocked.

Optic Information			Flaw Information							Blocker Information					Generate Blocker NCR
Beam	Optic Type	Optic SN	Flaw Id	Observed Size (mm)	Dwg X (mm)	Dwg Y (mm)	First Seen	Last Seen	Growing	Available Blockers	NCR Number	LOCOS Blocked	Image	Growth Chart	
B118	GDS	711336	26121570	0.244	75.7	149.8	FODI	N140915-003-999_140915_231005	1		NULL				<input type="checkbox"/>
B137	GDS	712184	17494304	0.200	132.5	60.6	FODI	N140915-003-999_140915_231005	1		NULL				<input type="checkbox"/>
B164	GDS	711257	24740856	0.223	186.4	282.7	FODI	N140915-003-999_140915_231005	1		NULL				<input type="checkbox"/>

Fig. 20. Sample display from the Blocker Advisor tool used to assign spot blockers to growing damage sites. Operators confirm the need for spot blockers by selecting one or more of the check boxes on the far right and submitting the results to launch automated implementation.

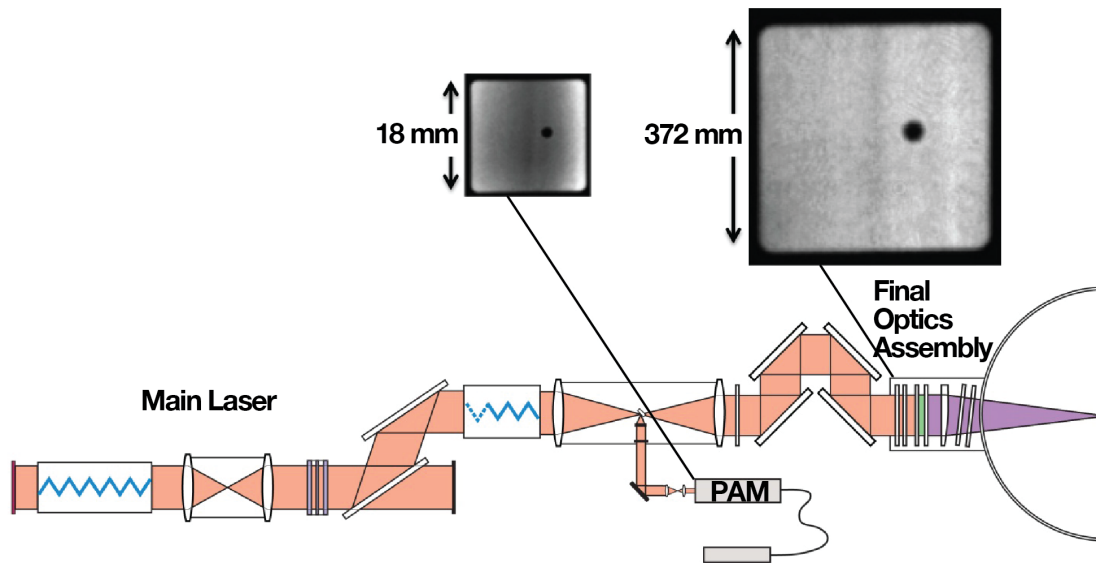


Fig. 21. Layout of the NIF laser system highlighting where programmable spot blockers are introduced in the PAM and their shadow images are relayed downstream at the FOA. Also shown are near-field images of the beam with a programmable spot blocker introduced at RP0 in the PAM and at a conjugate plane of the FOA.

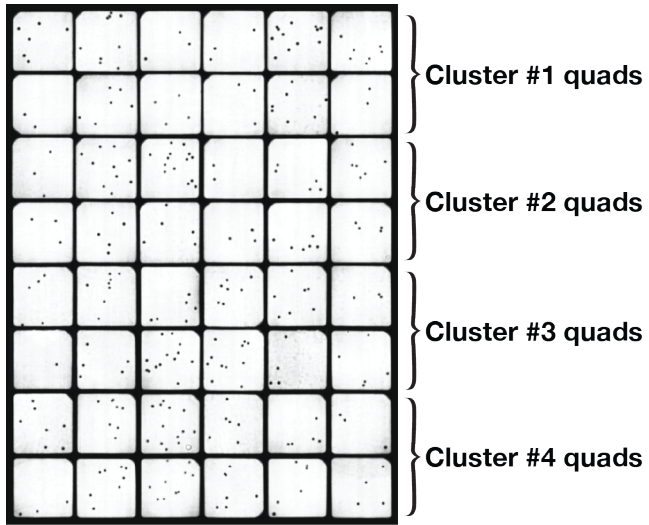


Fig. 22. High-energy 1ω beam profiles (one from each of the 48 quads) that display the number and location of all spot blockers in place for the full-system shot of June 8, 2012.

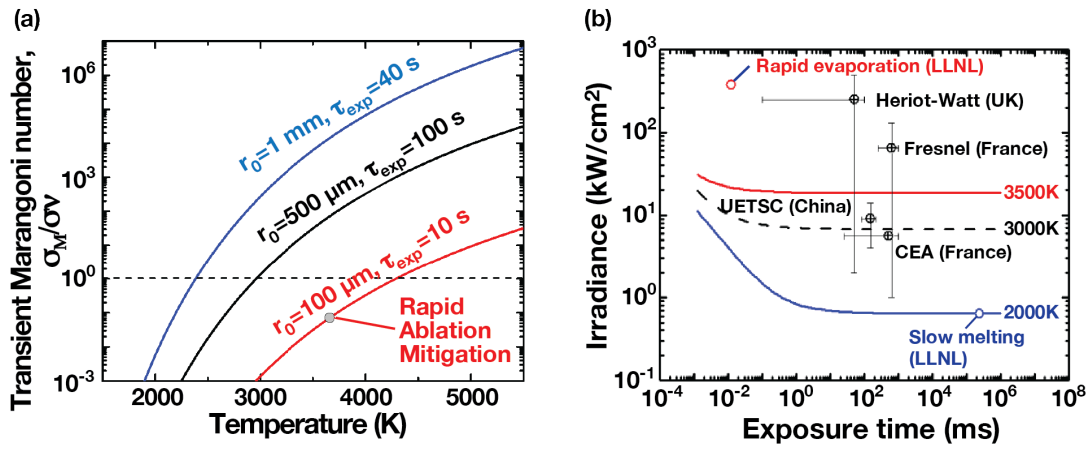


Fig. 23. (a) The calculated figure of merit—transient Marangoni number—as a function of peak temperature for different laser parameters (r_0 = beam diameter; τ_{exp} = pulse length). (b) Axial irradiance vs. laser exposure time for peak temperatures of 2000, 3000, and 3500 K, as predicted using analytic solutions to the linear heat-flow equation under laser heating.^{77, 78}

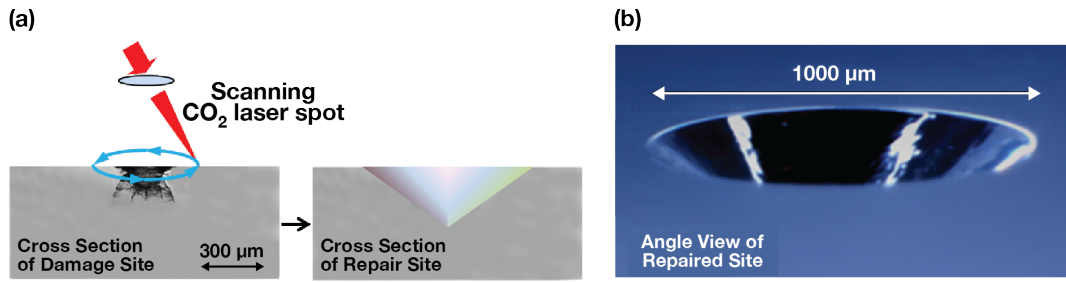


Fig. 24. Schematic showing the NIF laser damage repair process, which uses a scanned, pulsed, and focused CO₂ laser spot to evaporate a conical pit: (a) cross-section view and (b) angle view from top.

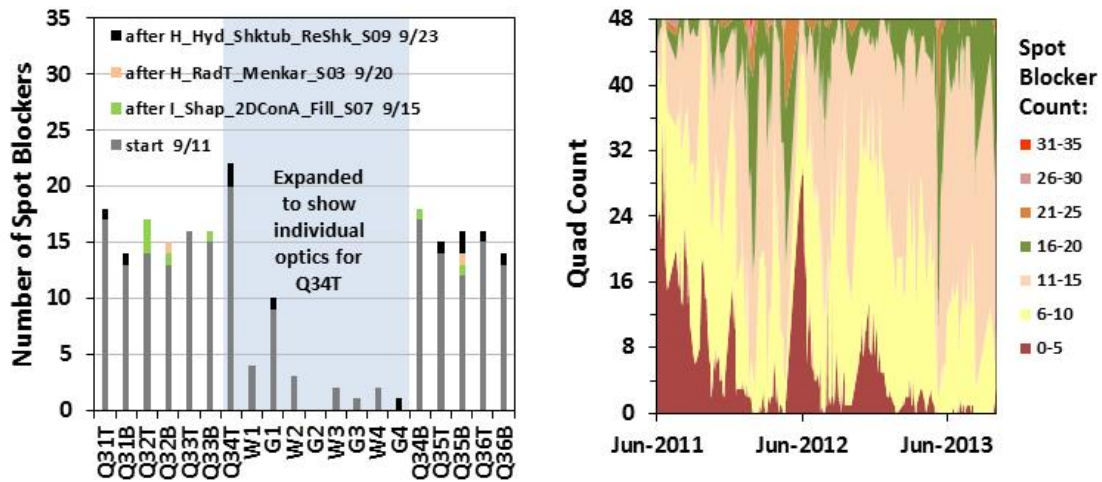


Fig. 25. (a) Detailed 2-week projection of spot blocker demand for Cluster 3 of the NIF laser, showing Quad 34T trending towards the spot blocker allocation limit of 24 per quad, due primarily to the GDS on Beam 341 (G1). (b) River plot showing management of spot blocker use over two years of operation.

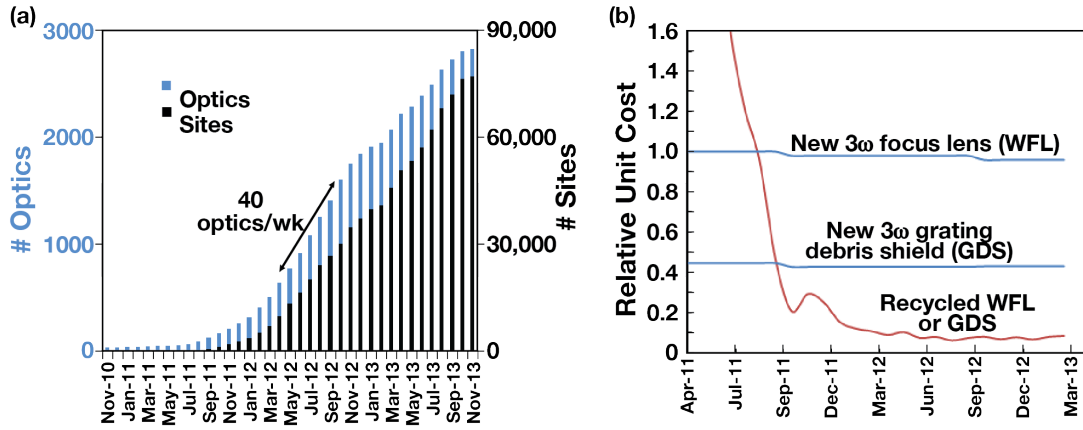


Fig. 26. (a) The cumulative number of optics processed and damage sites repaired in the recycle loop as a function of time; (b) relative unit cost of recycling GDS or WFL optics through the recycle loop as a function of time compared with the new optic cost.

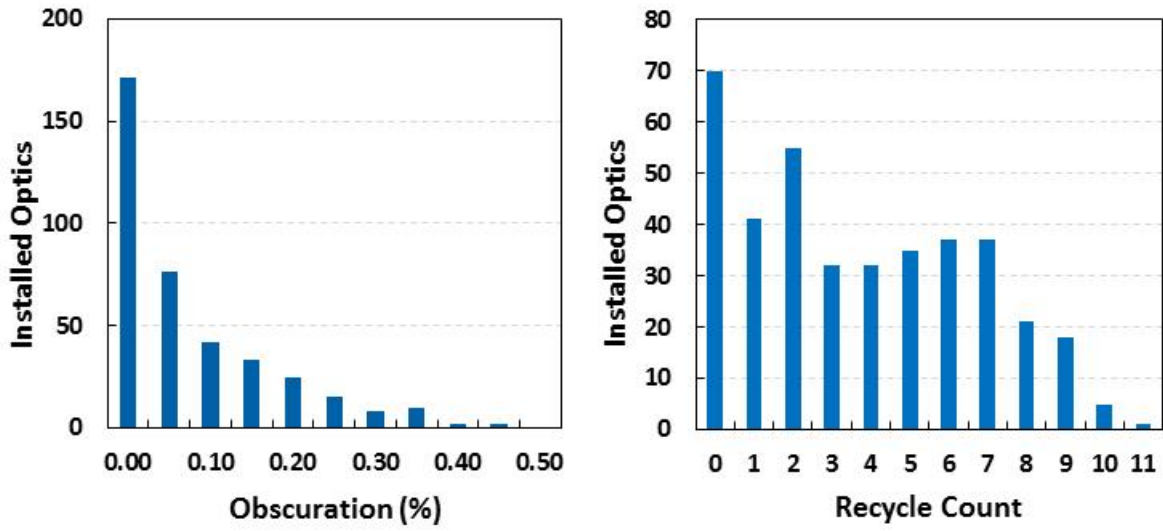


Fig. 27. (a) Population distribution of installed WFL and GDS optics with respect to recycle count and (b) total obscuration from mitigated damage sites.

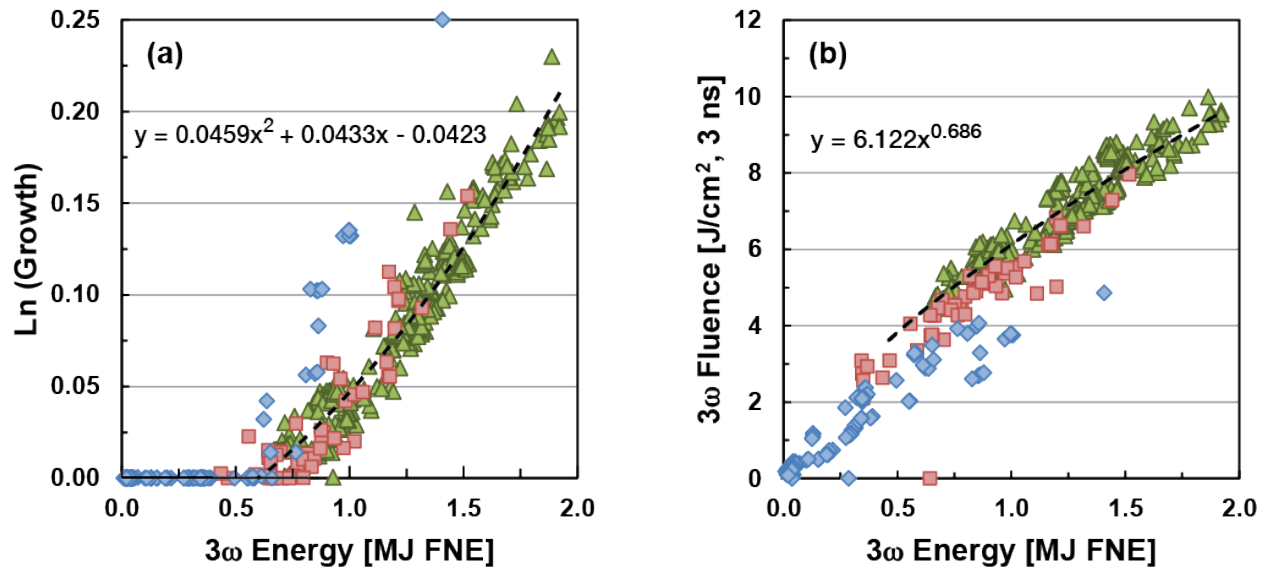


Fig. 28. (a) Average $\text{Ln}(\text{Growth})$ and (b) average 3-ns Gaussian equivalent fluence for NIF shots with ≥ 50 beams taken between Sept. 2011 and June 2014, plotted versus Full-NIF Equivalent (FNE) energy. Data is divided into three different FNE power ranges: $< 190\text{TW}$ (diamonds), 190 to 350TW (squares) and $> 350\text{TW}$ (triangles). Approximate fits to the higher power data set are indicated. Figure 28 (a) illustrates an important point; without one or the other of an operational ability to recycle damaged optics or the availability of optics with damage resistance well above the operating fluence range of the laser, the total output energy from the laser would be limited by damage growth to roughly less than 650 kJ per shot.

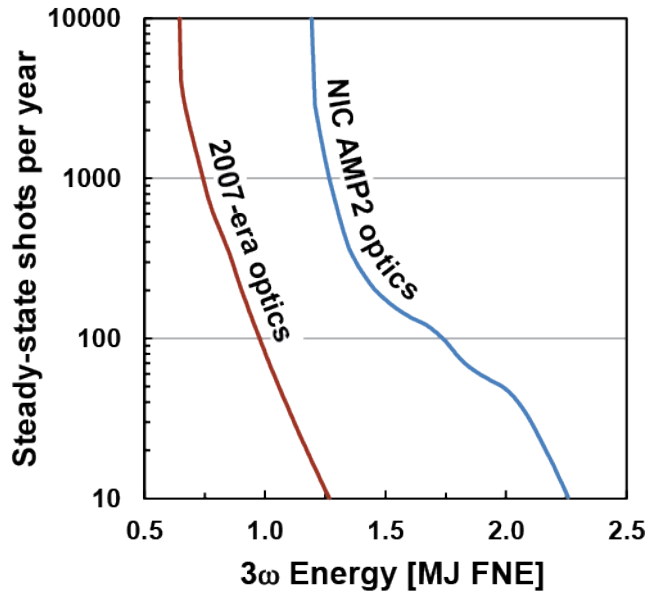


Fig. 29. Calculation of steady-state shot rate that can be supported by the optics recycle loop operating at capacities demonstrated during the NIC, as a function of laser operating point. Energies are those relevant for ignition-type pulses (see text). Curve on the right is modeled using optics with AMP2 damage characteristics as implemented during the NIC. For comparison, the curve on the left simulates the performance that would be expected for optics with 2007-era damage characteristics.

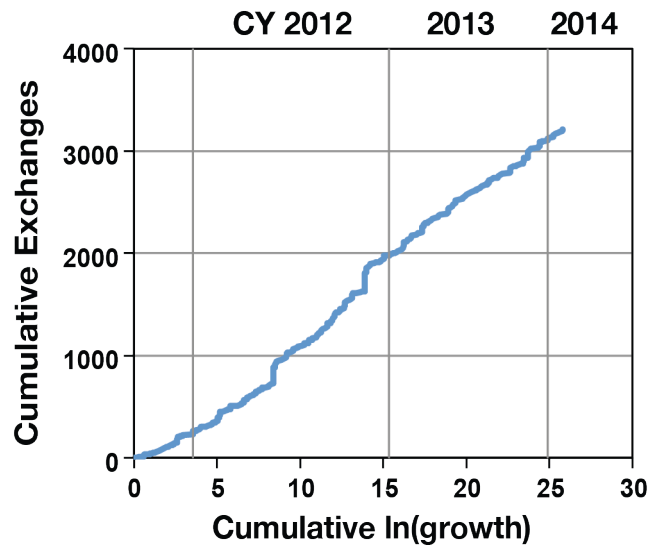


Fig. 30. Cumulative optics exchanges versus cumulative ln(growth) since September 2011.

Exchanges include both recycled and new or refinished optics.

VI. ACKNOWLEDGEMENTS

The authors gratefully acknowledge the many contributors who helped make the NIF optics recycle loop a reality, from developing the underlying science and technology to engineering and fielding the associated infrastructure, hardware, processes and operation. Wherever possible the contributions of these individuals are acknowledged by citations of their work: J. Adams, T. Alger, L. Auyang, A. Awwal, S. Azevedo, I. Bass, R. Beale, R. Beeler, W. Behrendt, R. Bettencourt, T. Biesiada, M. Bowers, M. Borden, S. Brereton, G. Brunton, S. Burns, J. Campbell, K. Carlisle, C. Carr, J. Chang, C. Choate, K. Christensen, R. Clark, S. Cohen, W. Collins, J. Comins, D. Cross, R. Darbee, J. Davis, A. Dawson, J.M. Di Nicola, S. Dixit, D. Dobson, V. Draggoo, S. Elhadj, C. Ellerbee, E. Elmido, C. Estes, J. Fair, R. Fallejo, M. Federov, M. Feit, R. Finucane, M. Flegel, C. Foxworthy, M. Franks, T. Frazier, S. Frieders, J. Gaylord, P. Geraghty, S. Glenn, W. Gourdin, G. Guss, R. Hackel, G. Hampton, R. Hawley, C. Haynam, M. Henesian, M. Hermann, J. Honig, D. Hopkins, J. Horner, R. House, W. House, H. Hui, S. Hunter, J. Jackson, M. Jackson, K. Jancaitis, G. Johnson, M. Johnson, K. Kasper, T. Kohut, E. Krieger, V. Lakamsani, L. Lane, G. Larkin, T. Laurence, Z. Liao, J. Liebman, K. Manes, B. Maranville, E. Marley, A. Marsh, C. Marshall, W. Massey, K. McCarty, D. McGuigan, J.B. Mcleod, N. Mehta, B. Merritt, P. Miller, M. Monticelli, E. Moses, R. Negres, M. Norton, M. O'Brien, C. Orth, T. Parham, A. Peer, J. Peterson, D. Potter, R. Prasad, K. Primdahl, D. Ravizza, F. Ravizza, B. Raymond, B. Rittmann, P. Rocha, M. Scanlan, J. Senecal, L. Seppala, M. Shaw, R. Shelton, L. Smith, R. Steele, J. Stolkein, C. Stolz, J. Tappero, M. Taranowski, R. Thacker, G. Tietbohl, D. VanBlarcom, D. Walmer, T. Weiland, B. Welday, C. Widmayer, W. Williams, J. Wolfe, N. Wong, B. Woods, T. Wulff, and S. Yang. We also thank the NIF senior management team for their guidance, encouragement and support: R. Al-Ayat, J. Atherton, P.

Baisden, G. Bonanno, L. Lagin, D. Larson, E. Moses, R. Patterson, R. Sawicki, V. Roberts, and B. Van Wonterghem.

This work performed under the auspices of the U.S. Department of Energy by Lawrence Livermore National Laboratory under Contract DE-AC52-07NA27344. Much of the fundamental science enabling the loop technologies was supported by the Laboratory Directed Research and Development (LDRD) Program.

REFERENCES

1. F. RAINER, R. BRUSASCO, J. CAMPBELL, F. DE MARCO, R. GONZALES, M. KOZLOWSKI, F. MILANOVICH, A. MORGAN, M. SCRIVENER, M. STAGGS, I. THOMAS, S. VELSKO, AND C. WOLFE, "Damage measurements on optical materials for use in high-peak-power lasers," *Proc. SPIE* **1438** (1989).
2. M. FEIT, F. GENIN, A. RUBENCHIK, L. SHEEHAN, S. SCHWARTZ, M. KOZLOWSKI, J. DIJON, P. GARREC, J. HUE, "Statistical description of laser damage initiation on NIF and LMJ optics at 355 nm," *Proc. SPIE* **3492** (1998).
3. M. NORTON, L. HRUBESH, Z. WU, E. DONOHUE, M. FEIT, M. KOZLOWSKI, D. MILAM, K. NEEB, W. MOLANDER, A. RUBENCHIK, W. SELL, P. WEGNER, "Growth of laser-initiated damage in fused silica at 351 nm," *Proc. SPIE* **4347**, 468 (2000)
4. C. CARR, M. MATTHEWS, J. BUDE, AND M. SPAETH, "The effect of laser pulse duration on laser-induced damage in KDP and SiO₂," *Proc. SPIE* **6403** (2006).
5. R. NEGRES, D. CROSS, Z. LIAO, M. MATTHEWS, AND C. CARR, "Growth model for laser-induced damage on the exit surface of fused silica under UV, ns laser irradiation," *Optics Express* **22**(4), 3824–3844 (2014).
6. T. SURATWALA, M. HANNA, E. MILLER, P. WHITMAN, I. THOMAS, P. EHRMANN, R. MAXWELL, AND A. BURNHAN, "Surface chemistry and trimethylsilyl functionalization of Stober silica sols," *J. Non-Cryst. Solids* **316**, 349–363 (2003).
7. I. THOMAS, "High laser damage threshold porous silica antireflective coating," *Applied Optics* **25**(9), 1481–1483 (1986).

8. T. SURATWALA, M. HANNA, AND P. WHITMAN, “Effect of humidity during the coating of Stober silica sols,” *Journal of Non-Crystalline Solids* **349**, 368–376 (2004).
9. P. WHITMAN et al., “Improved antireflection coatings for the NIF,” in *ICF Quarterly Report: Special Issue: Optics Technology for the National Ignition Facility*, UCRL-LR-105821-99-2 **9**(2), 163–176 (1999).
10. G. SOMMARGREN, “Phase shifting diffraction interferometry for measuring extreme ultraviolet optics,” in *OSA Trends in Optics and Photonics Vol. 4, Extreme Ultraviolet Lithography*, G Kubiak and D. Kania, Eds. (Optical Society of America, Washington, DC), 108–112 (1996).
11. D. PHILLION, “General methods for generating phase-shifting interferometry algorithms,” *Applied Optics* **36**, 8098–8115 (1997).
12. M. MONTICELLI, M. NOSTRAND, N. MEHTA, L. KEGELMEYER, M. JOHNSON, J. FAIR, AND C. WIDMAYER, “The HMDS coating flaw removal tool,” *Proc. SPIE* **7132** 0V 1–8 (2008).
13. W. CARR, J. BUDE, AND P. DEMANGE, “Laser-supported solid-state absorption fronts in silica,” *Phys. Rev. B: Condens. Matter* **82**, 184303 (2010).
14. W. CARR, J. TRENHOLME, AND M. SPAETH, “Effect of temporal pulse shape on optical damage,” *Appl. Phys. Lett.* **90**, 1 (2007).
15. R. PRASAD, J. BRUERE, J. HALPIN, P. LUCERO, S. MILLS, M. BERNACIL AND R. HACKEL, “Design of a production process to enhance optical performance of 3ω optics,” *Proc. SPIE* **5273** (2004).
16. T. LAURENCE, J. BUDE, N. SHEN, W. STEELE, AND S. LY, “Quasi-continuum photoluminescence: Unusual broad spectral and temporal characteristics found in

- defective surfaces of silica and other materials.” *Journal of Applied Physics* **115**, 083501 (2014).
17. P. MILLER, J. BUDE, T. SURATWALA, N. SHEN, T. LAURENCE, W. STEELE, J. MENAPACE, M. FEIT, AND L. WONG, “Fracture-induced subbandgap absorption as a precursor to optical damage on fused silica surfaces,” *Opt. Lett.* **35**(16), 2702–2704 (2010).
 18. T. LAURENCE, J. BUDE, N. SHEN, T. FELDMAN, P. MILLER, W. STEELE, AND T. SURATWALA, “Metallic-like photoluminescence and absorption in fused silica surface flaws,” *Appl. Phys. Lett.* **94**, 151114 (2009).
 19. T. SURATWALA, L. WONG, P. MILLER, M. FEIT, J. MENAPACE, R. STEELE, P. DAVIS, AND D. WALMER, “Sub-surface mechanical damage distributions during grinding of fused silica,” *Journal of Non-Crystalline Solids* **352**, 5601 (2006).
 20. J. MENAPACE, P. DAVIS, R. STEELE, L. WONG, T. SURATWALA, AND P. MILLER, “Utilization of magnetorheological finishing as a diagnostic tool for investigating the three-dimensional structure of fractures in fused silica,” *Proc. SPIE* **5991** doi: 10.1117/12.638840 (2005).
 21. P. MILLER, T. SURATWALA, L. WONG, M. FEIT, J. MENAPACE, P. DAVIS, AND R. STEELE, “The distribution of subsurface damage in fused silica,” *Proc. SPIE* **5991** doi:10.1117/12.638821 (2005).
 22. B. LAWN, *Fracture of Brittle Solids*, Second Edition, Cambridge Solid State Science Series (Cambridge University Press, New York, 1993).
 23. I.M. HUTCHINGS, “Tribology: Friction and Wear of Engineering Materials,” *Butterworth/Heinmann* (1992).

24. T. SURATWALA, R. STEELE, M. FEIT, L. WONG, P. MILLER, J. MENAPACE, AND P. DAVIS, “Effect of rogue particles on the sub-surface damage of fused silica during grinding/polishing,” *Journal of Non-Crystalline Solids* **354**, 2023–2037 (2008).
25. R. DYLLA-SPEARS, M. FEIT, P. MILLER, W. STEELE, T. SURATWALA, AND L. WONG, “Method for preventing agglomeration of charged colloids without loss of surface activity,” US Provisional Patent Application IL-12647 (Oct. 2012).
26. T. SURATWALA, W. STEELE, M. FEIT, R. DESJARDIN, D. MASON, R. DYLLA-SPEARS, L. WONG, P. MILLER, P. GERAGHTY, AND J. BUDE, “Method and system for convergent polishing,” US Patent Application 027512-006200US 61454893 (March 21, 2011).
27. J. MENAPACE, “Developing magnetorheological finishing (MRF) technology for the manufacture of large-aperture optics in megajoule class laser systems,” *Proc. SPIE* **7842W-1** doi: 10.1117/12.855603 (2010).
28. L. WONG, T. SURATWALA, M.D. FEIT, P.E. MILLER, R. STEELE, “The effect of HF/NH₄F etching on the morphology of surface fractures on fused silica,” *Journal of Non-Crystalline Solids* **355** 797–810 (2009).
29. T. SURATWALA, P. MILLER, M. FEIT, AND J. MENAPACE, “Scratch forensics,” *Optics and Photonics News* **12** (Sept. 2008).
30. M. FEIT, R. DESJARDIN, W. STEELE, AND T. SURATWALA, “Optimized pitch button blocking for polishing high-aspect-ratio optics,” *Applied Optics* **51** 8350–8359 (2012).

31. T. SURATWALA, R. STEELE, M. FEIT, R. DESJARDIN, AND D. MASON, "Convergent pad polishing of amorphous fused silica," *International Journal of Applied Glass Science* **3**(1), 14–28 (2012).
32. T. SURATWALA, M. FEIT, AND R. STEELE, "Toward deterministic material removal and surface figure during pad polishing of fused silica," *J. Am. Ceram. Soc.* **93**(5), 1326–1340 (2010).
33. T. SURATWALA, M. FEIT, R. STEELE, AND L. WONG, "Influence of temperature and material deposit on material removal uniformity during optical pad polishing," submitted to *J. Am. Ceram. Soc.* (2014).
34. T. SURATWALA, et. al., "Convergent polishing: a simple, rapid, full aperture polishing process of high quality optical flats and spheres," submitted to *Journal of Visualized Experiments* (2014).
35. R. DYLLA-SPEARS, L. WONG, P. MILLER, M. FEIT, W. STEELE, AND T. SURATWALA, "Charged micelle halo mechanism for agglomeration reduction in metal oxide polishing slurries," *Colloids and Surfaces A: Physicochem. Eng. Aspects* **447**, 32–43 (2014).
36. T. SURATWALA, et al., "Microscopic removal function and the relationship between slurry particle size distribution and workpiece roughness during pad polishing," *J. Am. Ceram. Soc.*, **91**(1), 81–91 (2014).
37. P. MILLER, T. SURATWALA, J. BUDE, N. SHEN, W. STEELE, T. LAURENCE, M. FEIT, AND L. WONG, "Methods for globally treating silica optics to reduce optical damage," US Patent Application 0079931A1 (April 7, 2011).

38. T. SURATWALA, P. MILLER, J. BUDE, W. STEELE, N. SHEN, M. MONTICELLI, M. FEIT, T. LAURENCE, M. NORTON, C. CARR, AND L. WONG, "HF-based etching processes for improving laser damage resistance of fused silica optical surfaces," *J. Am. Ceram. Soc.* **94**(2) 416–428 (2011).
39. T. LAURENCE, J. BUDE, N. SHEN, P. MILLER, W. STEELE, G. GUSS, J. ADAMS, L. WONG, M. FEIT, AND T. SURATWALA, "Ultrafast photoluminescence as a diagnostic for laser damage initiation," *Proc. SPIE* **7504** 750416 (2009).
40. K. KOKURA, M. TOMOZAWA, AND R. MACCRONE, "Defect formation in SiO₂ glass during fracture," *J. Non-Cryst. Solids* **111**, 269–276 (1989).
41. M. FEIT AND A. RUBENCHIK, "Influence of subsurface cracks on laser-induced surface damage," *Proc. SPIE* **5273**, 264 (2004).
42. F. GÉNIN, A. SALLEO, T. PISTOR, AND L. CHASE, "Role of light intensification by cracks in optical breakdown on surfaces," *J. Opt. Soc. Am. A* **18B** 2607–2616 (2001).
43. M. NORTON, C. CARR, D. CROSS, R. NEGRES, J. BUDE, W. STEELE, M. MONTICELLI, T. SURATWALA, "Determination of laser damage initiation probability and growth on fused silica scratches", *Proc. SPIE* **7842** (2010).
44. J. BUDE, P. MILLER, S. BAXAMUSA, N. SHEN, T. LAURENCE, W. STEELE, T. SURATWALA, L. WONG, W. CARR, D. CROSS and M. MONTICELLI, "High fluence laser damage precursors and their mitigation in fused silica," *Opt. Exp.* Vol. 22, 5839 (2014).
45. J. BUDE, P. MILLER, T. SURATWALA, T. LAURENCE, W. STEELE, S. BAXAMUSA, L. WONG, C. CARR, D. CROSS, M. MONTICELLI, M. FEIT, G.

- GUSS, "Silica laser damage mechanisms, precursors and their mitigation," SPIE Laser-induced damage in optical materials: 2014, 9237, 92307S, Sept. 2014.
46. S. BAXAMUSA, PE MILLER, L. WONG, R. STEETE, N. SHEN, J. BUDE, "Mitigation of organic laser damage precursors from chemical processing of fused silica," *Optics Express*, Vol. 22, 29568-29577, Dec 2014.
 47. J. HUNT, K. MANES, AND P. RENNARD, "Hot images from obscurations," *Appl. Opt.* **32** (1993).
 48. F. RAVIZZA, M. NOSTRAND, L. KEGELMEYER, R. HAWLEY, AND M. JOHNSON, "Process for rapid detection of fratricidal defects on optics using linescan phase differential imaging," *Proc. SPIE* **7504** doi:10.1117/12.836990 (2009).
 49. T. LAURENCE, J. BUDE, S. LY, N. SHEN, AND M. FEIT, "Extracting the distribution of laser damage precursors on fused silica surfaces for 351 nm, 3 ns laser pulses at high fluences (20–150 J/cm²)," *Optics Express* **20**(10), 11561–11573 (2012).
 50. C. CARR, D. CROSS, M. NORTON, AND R. NEGRES, "The effect of laser pulse shape and duration on the size at which damage sites initiate and the implications to subsequent repair," *Optics Express* **19**, A859–A864 (2011).
 51. C. CARR, M. FEIT, M. NOSTRAND, AND J. ADAMS, "Techniques for qualitative and quantitative measurement of aspects of laser-induced damage important for laser beam propagation," *Meas. Sci. Technol.* **17B**, 1958–1962 (2006).
 52. A. CONDER, J. CHANG, L. KEGELMEYER, et al., "Final optics damage inspection (FODI) for the National Ignition Facility," *Proc. SPIE* **7797**, 77970P (2010).
 53. A. CONDER et al., "Final optics damage inspection (FODI) for the National Ignition Facility," *Proc. SPIE* **6720**, 672010 (2008).

54. L. KEGELMEYER, R. CLARK, R. LEACH, D. MCGUIGAN, V. MILLER-KAMM, D. POTTER, J. SALMON, J. SENEAL, A. CONDER, M. NOSTRAND, AND P. WHITMAN, “Automated optics inspection analysis for NIF,” *Fusion Eng. Des.* **87**(12), 2120–2124, <http://dx.doi.org/10.1016/j.fusengdes.2012.09.017> (2012).
55. L. KEGELMEYER, P. FONG, S. GLENN, AND J. LIEBMAN, “Local area signal-to-noise ratio (LASNR) algorithm for image segmentation,” *Proc. SPIE* **6696**-2H doi: 10.1117/12.732493 (2007).
56. L. KEGELMEYER, J. SENEAL, A. CONDER, L. LANE, M. NOSTRAND, AND P. WHITMAN, “Optimizing blocker usage on NIF using image analysis and machine learning,” *ICALEPCS 2013*.
57. L. KEGELMEYER, “Applying Avatar Machine Learning to NIF Optics Inspection Analysis,” presented to Conference on Intelligent Data Understanding, p. 42, <https://c3.nasa.gov/dashlink/resources/221/> (October 6, 2010).
58. G. ABDULLA, L. KEGELMEYER, Z. LIAO, AND W. CARR, “Effective and efficient optics inspection approach using machine learning algorithms,” *Proc. SPIE* **7842**-1D doi: 10.1117/12.867648 (2010).
59. N. CHAWLA, L. HALL, K. BOWYER, AND W. KEGELMEYER, “Learning ensembles from bites: a scalable and accurate approach,” *Journal of Machine Learning Research* **5**, 421–451 (2004).
60. R. BEELER JR., A. CASEY, A. CONDER, R. FALLEJO, M. FLEGEL, M. HUTTON, K. JANCAITIS, V. LAKAMSANI, D. POTTER, S. REISDORF, J. TAPPERO, P. WHITMAN, W. CARR, AND Z. LIAO, “Shot planning and analysis tools on the NIF

project,” *Fusion Engineering Design* **87**(12), 2020–2024,
<http://dx.doi.org/10.1016/j.fusengdes.2012.09.007> (2012).

61. W. BLEHA, L. LIPTON, E. WIENER-AVNEAR, J. GRINBERG, P. REIF, D. CASASENT, H. BROWN, AND B. MARKEVITCH, “Application of the liquid crystal light valve to real-time optical data processing,” *Opt. Eng.* **17**, 371 (1978).
62. P. AUBOURG, J. HUIGNARD, M. HARENG, AND R. MULLEN, “Liquid crystal light valve using bulk monocrystalline $\text{Bi}_{12}\text{SiO}_{20}$ as the photoconductive material,” *Appl. Opt.* **21**, 3706–3712 (1982).
63. J. HEEBNER, M. BORDEN, P. MILLER, C. STOLZ, T. SURATWALA, P. WEGNER, M. HERMANN, M. HENESIAN, C. HAYNAM, S. HUNTER, K. CHRISTENSEN, N. WONG, L. SEPPALA, G. BRUNTON, E. TSE, A. AWWAL, M. FRANKS, E. MARLEY, K. WILLIAMS, M. SCANLAN, T. BUDGE, M. MONTICELLI, D. WALMER, S. DIXIT, C. WIDMAYER, J. WOLFE, J. BUDE, K. MCCARTY, AND J.-M. DINICOLA, “A programmable beam shaping system for tailoring the profile of high fluence laser beams,” *Proc. SPIE* **7842-1C** (2010).
64. J. HEEBNER, M. BORDEN, P. MILLER, S. HUNTER, K. CHRISTENSEN, M. SCANLAN, C. HAYNAM, P. WEGNER, M. HERMANN, G. BRUNTON, E. TSE, A. AWWAL, N. WONG, L. SEPPALA, M. FRANKS, E. MARLEY, K. WILLIAMS, T. BUDGE, M. HENESIAN, CH. STOLZ, T. SURATWALA, M. MONTICELLI, D. WALMER, S. DIXIT, C. WIDMAYER, J. WOLFE, J. BUDE, K. MCCARTY, AND J.-M. DINICOLA, “Programmable beam spatial shaping system for the National Ignition Facility,” *Proc. SPIE* **7916** (2011).

65. S. BAHK, J. ZUEGEL, J. FIENUP, AND C. WIDMAYER, "Spot-shadowing optimization to mitigate damage growth in a high-energy-laser amplifier chain," *Applied Optics* **47**, 6586–6593 (2008).
66. L. HRUBESH, M. NORTON, W. MOLANDER, E. DONOHUE, S. MARICLE, B. PENETRANTE, R. BRUSASCO, W. GRUNDLER, J. BUTLER, J. CARR, R. HILL, L. SUMMERS, M. FEIT, A. RUBENCHIK, M. KEY, P. WEGNER, A. BURNHAM, L. HACKEL, AND M. KOZLOWSKI, "Methods for mitigating surface damage growth on NIF final optics," *Proc. SPIE* **4679**, 23–33 (2002).
67. R. BRUSASCO, B. PENETRANTE, J. BUTLER, AND L. HRUBESH, "Localized CO₂ laser treatment for mitigation of 351 nm damage growth on fused silica," *Proc. SPIE* **4679**, 40–47 (2002).
68. A. BURNHAM, L. HACKEL, P. WEGNER, T. PARHAM, L. HRUBESH, B. PENETRANTE, P. WHITMAN, S. DEMOS, J. MENAPACE, M. RUNKEL, M. FLUSS, M. FEIT, M. KEY, AND T. BIESIADA, "Improving 351-nm damage performance of large-aperture fused silica and DKDP optics," *Proc. SPIE* **4679**, 173–185 (2002).
69. E. MENDEZ, K.M. NOWAK, H.J. BAKER, F.J. VILLARREAL, AND D.R. HALL, "Localized CO₂ laser damage repair of fused silica optics," *Applied Optics* **45**, 5358–5367 (2006).
70. G. GUSS, I. BASS, V. DRAGGOO, R. HACKEL, S. PAYNE, M. LANCASTER, AND P. MAK, "Mitigation of growth of laser initiated surface damage in fused silica using a 4.6- μ m wavelength laser," *Proc. SPIE* **6403-0M** (2007).
71. S. YANG, M. MATTHEWS, S. ELHADJ, D. COOKE, G. GUSS, V. DRAGGOO, AND P. WEGNER, "Comparing the use of mid-infrared versus far-infrared lasers for

- mitigating damage growth on fused silica,” *Appl. Opt.* **49**, 2606–2616
<http://ao.osa.org/abstract.cfm?URI=ao-49-14-2606> (2010).
72. P. BOUCHUT, L. DELRIVE, D. DECRUPPE, AND P. GARREC, “Local re-fusion of silica, by a continuous CO₂ laser, for the mitigation of laser damage growth,” *Optical Fabrication, Testing, and Metrology* **5252**, 122–130 (2004).
73. I. BASS, G. GUSS, M. NOSTRAND, AND P. WEGNER, “An improved method of mitigating laser induced surface damage growth in fused silica using a rastered, pulsed CO₂ laser,” *Proc. SPIE* **7842** (2010).
74. I. BASS, V. DRAGGOO, G. GUSS, R. HACKEL, AND M. NORTON, “Mitigation of laser damage growth in fused silica NIF optics with a galvanometer scanned CO₂ laser,” *Proc. SPIE* **6261** (2006).
75. I. BASS, G. GUSS, AND R. HACKEL, “Mitigation of laser damage growth in fused silica with a galvanometer scanned CO₂ laser,” *Proc. SPIE* **5991** (2005).
76. J. ADAMS, M. BOLOURCHI, J. BUDE, G. GUSS, M. MATTHEWS, AND M. NOSTRAND, “Results of applying a non-evaporative mitigation technique to laser-initiated surface damage on fused silica,” *Proc. SPIE* **7842** (2010).
77. S. YANG, M. MATTHEWS, S. ELHADJ, V. DRAGGOO, AND S. BISSON, “Thermal transport in CO₂ laser irradiated fused silica: in situ measurements and analysis,” *J. Appl. Phys.* **106**, 1031061–1031067 (2009).
78. S. ELHADJ, M. MATTHEWS, S. YANG, D. COOKE, J. STOLKEN, R. VIGNES, V. DRAGGOO, AND S. BISSON, “Determination of the intrinsic temperature dependent thermal conductivity from analysis of surface temperature of laser irradiated materials,” *Appl. Phys. Lett.* **96**, 071110 (2010).

79. R. RAMAN, M. MATTHEWS, J. ADAMS, AND S. DEMOS, "Monitoring annealing via CO₂ laser heating of defect populations on fused silica surfaces using photoluminescence microscopy," *Optics Express* **18**, 15207–15215
<http://www.opticsexpress.org/abstract.cfm?URI=oe-18-14-15207> (2010).
80. M. MATTHEWS, J. STOLKEN, R. VIGNES, M. NORTON, S. YANG, J. COOKE, G. GUSS, AND J. ADAMS, "Residual stress and damage-induced critical fracture on CO₂ laser treated fused silica," *Proc. SPIE* **7504** (2009).
81. L. GALLAIS, P. CORMONT, and J.-L. RULLIER, "Investigation of stress induced by CO₂ laser processing of fused silica optics for laser damage growth mitigation," *Opt. Express* **17**(26), 23488-23501 (2009).
82. M. MATTHEWS, I. BASS, G. GUSS, C. WIDMAYER, AND F. RAVIZZA, "Downstream intensification effects associated with CO₂ laser mitigation of fused silica," *Proc. SPIE* **6720** (2007).
83. R. VIGNES, T. SOULES, J. STOLKEN, R. SETTGAST, S. ELHADJ, AND M. MATTHEWS, "Thermomechanical modeling of laser-induced structural relaxation and deformation of glass: volume changes in fused silica at high temperatures," *J. Am. Ceram. Soc.* **96**, 137–145, <http://dx.doi.org/10.1111/jace.12110> (2013).
84. M. MATTHEWS, R. VIGNES, D. COOKE, S. YANG, AND J. STOLKEN, "Analysis of microstructural relaxation phenomena in laser-modified fused silica using confocal Raman microscopy," *Opt. Lett.* **35**, 1311–1313 (2010).
85. N. SHEN, M. MATTHEWS, J. FAIR, J. BRITTEN, H. NGUYEN, D. COOKE, S. ELHADJ, AND S. YANG, "Laser smoothing of sub-micron grooves in hydroxyl-rich fused silica," *Appl. Surf. Sci.* **256**, 4031–4037 (2010).

86. S. ELHADJ, M. MATTHEWS, S. YANG, AND D. COOKE, “Evaporation kinetics of laser heated silica in reactive and inert gases based on near-equilibrium dynamics,” *Optics Express* **20**, 1575–1587 (2012).
87. J. FOLTA, et al., “Mitigation of laser damage on the National Ignition Facility optics in volume production,” *Proc. SPIE* **8885** (2013).
88. Z. LIAO, J. HUBEL, J. TRENHOLME, AND C. CARR, “Modeling max-of-N fluence distribution using measured shot-to-shot beam contrast,” *Applied Optics* **50**, 3547–3552 (2011).
89. C. CARR, Z. LIAO, M. NORTON, AND R. NEGRES, “Effect of laser pulse shape on optical damage growth rate,” LLNL internal memorandum NIF-0175664 (2014), to be published.